ENCLOSURE 4

MHI Non-Proprietary Document

L5-04GA567, Evaluation of Stability Ratio for Return to Service

(Non-Proprietary)

Non-proprietary Version

[ ] (1/149)

San Onofre Nuclear Generating Station, Unit 2 & 3
REPLACEMENT STEAM GENERATORS

Evaluation of Stability Ratio for Return to Service

Supplier Status Stamp

VPL No:	SO23-617-1-M1539	Rev No: 0	QC: N/A

☐ DESIGN DOCUMENT ORDER NO. 800873488
☒ REFERENCE DOCUMENT–INFORMATION ONLY ☐ VIRP IOM MANUAL

MFG MAY PROCEED: ☐ YES ☐ NO ☒ N/A

STATUS - A status is required for design documents and is optional for reference documents. Drawings are reviewed and approved for arrangements and conformance to specification only. Approval does not relieve the submitter from the responsibility of adequacy and suitability of design, materials, and/or equipment represented.

☐ 1. **APPROVED**
☐ 2. **APPROVED EXCEPT AS NOTED** - Make changes and resubmit.
☐ 3. **NOT APPROVED** - Correct and resubmit for review. NOT for field use.

APPROVAL: (PRINT / SIGN / DATE)

RE: D. Calhoun 10/1/12

FLS:

Other:

SCE DE(123) 6 REV. 3 07/11 REFERENCE: SO123-XXIV-37.8.26

Purchase Order No.	4500024051
Specification No.	SO23-617-01R3

CONTENT		REMARKS	PURCHASER	ORDER No.	DATE	Nuclear Plant Component Designing Department Steam Generator Designing Section	
DESCRIPTION	- PAGE			ITEM No.	REFERENCE		
	- SHEET		Edison (MNES)	2591012		APPROVED BY	
TOTAL	149 PAGE			1000		CHECKED BY	
						DESIGNED BY	
						DRAWN BY	—
						—	—
						ISSUE DATE	

Distribution																PM(S)	COPY
Edison																1	1

DWG. No. L5-04GA567 Rev.No. 6

MITSUBISHI HEAVY INDUSTRIES, LTD.

Revision History

Document No.L5-04GA567

No.	Revision	Date	Approved	Checked	Prepared
0	Initial issue	See cover sheet			
1	-Revised in accordance with SCE comments of RSG-SCE/MHI-12-5722. -Added the evaluation of out of plane FEI.				
2	Revised in accordance with SCE comments of RSG-SCE/MHI-12-5729.				
3	-Revised the calculation method of the virtual added mass of tube in Sec. 4.1(5).				
4	- Added Attachment-5 to evaluate the stability ratio of the tube which has tube-to-tube wear at 70% thermal power				
5	- Revised Attachment-5 to evaluate the effect of type J stabilizer on stability ratio of the tube which has tube-to-tube wear at 70% thermal power - Added Attachment-6 to evaluate the uncertainty of calculated stability ratio				
6	-Revised in accordance with SCE comments of RSG-SCE/MHI-12-5769 -Revised stability ratios due to the change of stabilizer type (Type J) -Revised out-of-plane FEI analysis results in Sec.2 and 8				

Table of Contents

1. Purpose

The purpose of this document is to perform parametric calculations of stability ratios for the selected (limiting) tubes as a function of the number of consecutive inactive AVB support points and the reactor (thermal) power level. This calculation is performed in support of SONGS Units 2 return to service.

2. Conclusion

By considering numbers of inactive support points as the parameter for the case study, the following results are obtained.

2.1 Stability ratio of out of plane FEI

2.1.1 Assuming all support points active

With all AVB supports active, the stability ratios are less than 1.0 for all analyzed tubes, for the reactor power levels up to, and including, 100% with no plugging.

Table 2.1-1 Stability Ratio with All Active Support Points for 2A SG

Case		Thermal Power	
Row	Column	70	100 (No Plug)
80	70		
80	80		
100	70		
100(*)	80(*)		
120	70		
120	80		
95(*)	85(*)		
125	85		
138	84		

6

Note(*): Plugged tube with Type J stabilizer

2.1.2 Assuming 1 support points inactive

With 1 AVB supports inactive, the stability ratios are less than 1.0 for all analyzed tubes, for the reactor power levels up to, and including, 70%

Table 2.1-2 Stability Ratio with 1 Inactive Support Point for 2A SG

Case		Thermal Power	
Row	Column	70	100 (No Plug)
80	70		
80	80		
100	70		
100(*)	80(*)		
120	70		
120	80		
95(*)	85(*)		
125	85		
138	84		

6

Note(*): Plugged tube with Type J stabilizer

2.2 Stability ratio of in-plane FEI

2.2.1 Assuming 6 support points inactive

With 6 consecutive AVB supports inactive, the stability ratios are less than 1.0 for all analyzed tubes, for the reactor power levels up to, and including, 90%.

Table 2.2-1 Stability Ratio with 6 Consecutive Inactive Support Points for 2A SG

Case		Thermal Power						
Row	Column	50	60	70	80	90	100	100 (No Plug)
80	70							
80	80							
100	70							
100(*)	80(*)							
120	70							
120	80							
95(*)	85(*)							
125	85							
138	84							

Note(*): Plugged tube with Type J stabilizer

2.2.2 Assuming 8 support points inactive

With 8 consecutive AVB supports inactive, the stability ratios are less than 1.0 for all analyzed tubes, for the reactor power levels up to, and including, 80%.

Table 2.2-2 Stability Ratio with 8 Consecutive Inactive Support Points for 2A SG

Case		Thermal Power						
Row	Column	50	60	70	80	90	100	100 (No Plug)
80	70							
80	80							
100	70							
100(*)	80(*)							
120	70							
120	80							
95(*)	85(*)							
125	85							
138	84							

Note(*): Plugged tube with Type J stabilizer

2.2.3 Assuming 10 support points inactive

With 10 consecutive AVB supports inactive, the stability ratios are less than 1.0 for all analyzed tubes, for the reactor power levels up to, and including, 80% after plugging.

Table 2.2-3 Stability Ratio with 10 Consecutive Inactive Support Points for 2A SG

Case		Thermal Power						
Row	Column	50	60	70	80	90	100	100 (No Plug)
80	70							
80	80							
100	70							
100(*)	80(*)							
120	70							
120	80							
95(*)	85(*)							
125	85							
138	84							

Note(*): Plugged tube with Type J stabilizer

2.2.4 Assuming 12 support points inactive

With 12 consecutive AVB supports inactive, the stability ratios are less than 1.0 for all analyzed tubes, for the reactor power levels up to, and including, 60%.

Table 2.2-4 Stability Ratio with 12 Consecutive Inactive Support Points for 2A SG

Case		Thermal Power						
Row	Column	50	60	70	80	90	100	100 (No Plug)
80	70							
80	80							
100	70							
100(*)	80(*)							
120	70							
120	80							
95(*)	85(*)							
125	85							
138	84							

6 6 6

Note(*): Plugged tube with Type J stabilizer

2.2.5 TTW tubes in Unit-2

The stability ratios of TTW (tube-to-tube wear) tubes with type J stabilizer (split stabilizers) in Unit-2 were evaluated and confirmed to be less than 1.0 as shown in Attachment-5. 6

3. Nomenclature

Symbol	Unit	Definition
E	psi	Modulus of elasticity of tube
FEI	-	Fluid elastic instability
G	psi	Shear modulus of tube
T_{av}	°F	Primary side average temperature
T_S	°F	Secondary side temperature
D_i	in	Tube inside diameter
D_o	in	Tube outside diameter
P	in	Tube pitch
ρ_i	lbm/ft^3	Density of water inside the tube
ρ_t	lbm/ft^3	Density of tube material
ρ_o	lbm/ft^3	Average density of water outside the tube
t	in	Tube thickness
m	lbm/ft	Tube mass distribution per unit length
m_v	lbm/ft	Virtual added mass per unit length
h	-	Damping ratio
h_s	-	Structural damping ratio
h_{TP}	-	Two phase damping ratio
h_v	-	Viscous damping ratio
h_{SF}	-	Squeeze film damping ratio
K	-	Critical factor
MHI	-	Mitsubishi Heavy Industries
m_0	lbm/ft	Average tube mass per unit length
U_c	ft/s	Critical flow velocity
f	Hz	Tube natural frequency
δ	-	Logarithmic decrement
U_{en}	ft/s	Nth mode effective flow velocity
Φ(x)	-	Vibration mode
$\Phi_n(x)$	-	Nth vibration mode
ρ , $\rho(x)$	lbm/ft^3	Fluid density distribution of water outside the tube in tube axis direction
U, U(x)	ft/s	Flow velocity distribution orthogonal to tube axis in tube axis direction
x	ft	Coordinate component along tube axis
L	ft	Tube length
SCE	-	Southern California Edison
SR, SR_n	-	(Nth mode) Stability ratio

4. Assumption

4.1 Modeling assumption

(1) Nominal tube thickness and nominal tube length are used in the evaluation model because the effect of the tolerances of these dimensions on the natural frequency is negligible.

(2) Contact condition between tube and tube support plate is pin-supported. Fixed supported condition at tubesheet is added.

(3) Contact condition between tube and active support points by the anti-vibration bar (AVB) is pin-supported.

(4) Modulus of elasticity of tube is interpolated based on the tube average temperature of $\frac{T_{av}+T_s}{2}$ from table of ASME Boiler and Pressure Vessel Code, Sec II, Materials, 1998 Edition, 2000 addenda (Ref.1).

Where,

T_{av} : Primary side average temperature (°F)

T_s : Secondary side saturation temperature (°F)

(5) Tube has the virtual added mass due to the fluid-structure interaction (FSI) effect. The virtual added mass in each region of the tube (the straight regions between TSPs and U-bend region) is calculated by using the following formula (Ref.24).

$$m_v = \frac{\pi D_o^2 \rho_o}{4}\left\{\frac{(D_e/D_o)^2+1}{(D_e/D_o)^2-1}\right\} \text{(lbm/ft)} \quad \cdots\cdots (1)$$

$$D_e/D_o = \left(1+\frac{1}{2}P/D_o\right)P/D_o \quad \cdots\cdots (2)$$

Where,

m_v : Virtual added mass per unit length due to FSI effect

ρ_o : Average water density outside the tube of each region obtained from ATHOS analysis

D_o : Tube outside diameter

P : Tube pitch

(6) Number of inactive AVB support points is a parameter for this case study. Consecutive 12 , 10 (B01 to B10), 8 (B01 to B08) and 6 (B01 to B06) inactive support points biased to the hot side are assumed for the evaluation of the stability ratio of in-plane FEI. All active support points and 1 inactive support point are assumed for the evaluation of the stability ratio of out of plane FEI. The location of 1 inactive support is determined based on hydraulic pressure, void fraction and support span of each evaluated tube. The inactive support will be one of the 2 supports at the span with the highest amplitude, whichever that has a higher hydraulic pressure. The maximum stability ratio in each inactive support location is shown as the result of the stability ratio with 1 inactive support.

(7) Type J stabilizers are assumed to be installed for all plugged tubes which have AVB wear indications. The additional structural damping ratio due to Type J stabilizer (split stabilizers installed to 60 degrees in the U-bend region at the both of hot and cold side) is assumed to be [ ] which is based on the MHI test results of the medium amplitude (see Ref. 32 and Attachment-1 for details). 6

4.2 Open item

There is no open item remaining.

5. Acceptance Criteria

The stability ratio against fluid elastic instability shall be less than 1.0. The analysis is performed in accordance with the procedures given in ASME code section III Appendix N-1330 (Ref.2).

6. Design Input

6.1 Geometry of tube bundle region

Tube bundle consists of thermally treated Alloy 690 U-tubes which are supported in[ ]triangular pitch arrangement by the tube sheet, seven tube support plates, and six sets of anti-vibration bars (AVBs). Tube support plates (TSPs) have trifoil tube holes.

All the contacting support structures above the tube sheet are made of 405 stainless steel (SA-240 Type 405 Stainless steel) .

Nominal dimension of tube, TSPs and AVBs are listed in Table 6-1. The applicable design drawings to be referred are listed in Table 6-2.

Table 6-1 Nominal dimensions of tubes, TSPs, and AVBs

Part	Item	Value
Tubes	Material	Thermally treated SB-163 UNS N06690
	Outside diameter	0.75 in
	Thickness	0.043 in
	Number of tubes	9727
	Tube pitch	1.0 in
	Tube arrangement	Triangular
TSPs	Material	SA-240 Type 405
	Thickness	
	Number of TSPs	
	Tube support span (between TSP centrals)	
	Tube support span (from TS to No.1 TSP)	
AVBs	Material	SA-479 Type 405
	Type	
	Thickness	
	Width	
Stabilizer	Unit weight	

6

Table 6-2 Applicable design drawings (Ref.3 to 20)

Drawing No.	Title
L5-04FU001	COMPONENT AND OUTLINE DRAWING 1/3
L5-04FU002	COMPONENT AND OUTLINE DRAWING 2/3
L5-04FU003	COMPONENT AND OUTLINE DRAWING 3/3
L5-04FU021	TUBE SHEET AND EXTENSION RING 1/3
L5-04FU022	TUBE SHEET AND EXTENSION RING 2/3
L5-04FU023	TUBE SHEET AND EXTENSION RING 3/3
L5-04FU051	TUBE BUNDLE 1/3
L5-04FU052	TUBE BUNDLE 2/3
L5-04FU053	TUBE BUNDLE 3/3
L5-04FU111	AVB ASSEMBLY 1/9
L5-04FU112	AVB ASSEMBLY 2/9
L5-04FU113	AVB ASSEMBLY 3/9
L5-04FU114	AVB ASSEMBLY 4/9
L5-04FU115	AVB ASSEMBLY 5/9
L5-04FU116	AVB ASSEMBLY 6/9
L5-04FU117	AVB ASSEMBLY 7/9
L5-04FU118	AVB ASSEMBLY 8/9
L5-04FU119	AVB ASSEMBLY 9/9

6.2 Thermal and hydraulic flow of steam generator secondary side

The basic parameters for the thermal hydraulic analysis of unit-2 and 3 steam generators are shown in Table 6.2-1 to 6.2-4. As discussed in ATHOS analysis report (Ref. 22), the larger number of the plugged tubes of unit-2 (305 tubes for 2A) is used for the FEI evaluation. The flow characteristics of the tubes listed in Table 7.2-1 are obtained from ATHOS/SGAP analysis (See Ref.21 and 22 for detail) and used for the vibration analysis.

The distributions of flow gap velocity normal to the in-plane direction of the tube, flow density and void fraction are shown in Fig.6.2-3 to 6.2-11. Several of the flow gap velocity distributions indicate negative flow velocities at lower thermal power on the cold leg side since the water flow is more likely to go downward on the cold leg side because the circulation ratio is higher and the water flow rate compared with steam flow rate at lower thermal power conditions is greater than higher thermal power condition.

As shown in Section 7, the effective flow velocity U_e is calculated as function of the square of flow velocity and mode shape in order to evaluate the actual tube vibration which is multi degrees of freedom system with beam type of vibration modes. Therefore, there is no adverse effect of negative flow velocity.

Table 6.2-1 Basic parameters for calculation for 2A SG evaluation after plugging

Case	50%	60%	70 %	80 %	90 %	100 %	100 % with no plugging
Plugging*6	305	305	305	305	305	305	0
Thermal power (MWt)	869.5 (50%)	1041.4 (60%)	1213.3 (70%)	1385.2 (80%)	1557.1 (90%)	1729 (100%)	1729
RCS flow rate (gpm) *1	206,695	206,695	206,695	206,695	206,695	206,695	209,880
T_{hot} (Tsg-in) (°F)							
$T_{sg\text{-}out}$ (°F)*2							
T_{cold} (°F)*2							
Saturation Steam Pressure (psia)							
Fouling Factor ($ft^2hr°F$ /Btu)							
$T_{feedwater}$ (°F)							
Circulation Ratio							
Steam Mass Flow (lb/hr)							
Feed Water Mass Flow (lb/hr)*3							
Blowdown flow rate (gpm)							

Note *1: Obtained by interpolating the flow rate of 0% plugging and 8% plugging.

*2: RCS flow temperature at SG outlet is assumed to be 0.3°F lower than that at RV inlet. The 0.3°F temperature increase between the SG outlet and RV inlet is caused by heat input from the reactor coolant pump.

*3: Feedwater mass flow rate is the sum of the blowdown flow rate and the steam mass flow based on heat balance calculation.

*4: Calculated by interpolating the data of other cases.

*5: Assumed to be the same as Unit-3.

*6: As discussed in ATHOS analysis report (Ref. 22), the larger number of unit-2 (305 tubes for 2A) is used for the evaluation. Fig.6.2-1 shows the address of the plugged tubes of 2A SG. Since ATHOS can only create a symmetrical half model of the tube bundle in reference to the center column of the SG, the asymmetrical plugged tubes cannot be modeled. Therefore the plugged tubes are assumed to be overlapped as shown in Fig.6.2-2.

Table 6.2-2 Basic parameters for calculation for 2B SG evaluation after plugging

Case	50%	60%	70 %	80 %	90 %	100 %	100 % with no plugging
Plugging*6	205	205	205	205	205	205	0
Thermal power (MWt)	869.5 (50%)	1041.4 (60%)	1213.3 (70%)	1385.2 (80%)	1557.1 (90%)	1729 (100%)	1729
RCS flow rate (gpm) *1	207,726	207,726	207,726	207,726	207,726	207,726	209,880
T_{hot} (Tsg-in) (°F)							
$T_{sg\text{-}out}$ (°F)*2							
T_{cold} (°F)*2							
Saturation Steam Pressure (psia)							
Fouling Factor ($ft^2hr°F$ /Btu)							
$T_{feedwater}$ (°F)							
Circulation Ratio							
Steam Mass Flow (lb/hr)							
Feed Water Mass Flow (lb/hr)*3							
Blowdown flow rate (gpm)							

Note *1: Obtained by interpolating the flow rate of 0% plugging and 8% plugging.

*2: RCS flow temperature at SG outlet is assumed to be 0.3°F lower than that at RV inlet. The 0.3°F temperature increase between the SG outlet and RV inlet is caused by heat input from the reactor coolant pump.

*3: Feedwater mass flow rate is the sum of the blowdown flow rate and the steam mass flow based on heat balance calculation.

*4: Calculated by interpolating the data of other cases.

*5: Assumed to be the same as Unit-3.

*6: As discussed in ATHOS analysis report (Ref. 22), the larger number of unit-2 (305 tubes for 2A) is used for the evaluation. Fig.6.2-1 shows the address of the plugged tubes of 2A SG.

Table 6.2-3 Basic parameters for calculation for 3A SG evaluation after plugging

Case	50%	60%	70 %	80 %	90 %	100 %	100 % with no plugging
Plugging*4	387	387	387	387	387	387	0
Thermal power (MWt)	869.5 (50%)	1041.4 (60%)	1213.3 (70%)	1385.2 (80%)	1557.1 (90%)	1729 (100%)	1729
RCS flow rate (gpm) *1	205,901	205,901	205,901	205,901	205,901	205,901	209,880
T_{hot} (Tsg-in) (°F)							
$T_{sg\text{-}out}$ (°F)*2							
T_{cold} (°F)*2							
Saturation Steam Pressure (psia)							
Fouling Factor ($ft^2hr°F$ /Btu)							
$T_{feedwater}$ (°F)							
Circulation Ratio							
Steam Mass Flow (lb/hr)							
Feed Water Mass Flow (lb/hr)*3							
Blowdown flow rate (gpm)							

Note

*1: Obtained by interpolating the flow rate of 0% plugging and 8% plugging.

*2: RCS flow temperature at SG outlet is assumed to be 0.3°F lower than that at RV inlet. The 0.3°F temperature increase between the SG outlet and RV inlet is caused by heat input from the reactor coolant pump.

*3: Feedwater mass flow rate is the sum of the blowdown flow rate and the steam mass flow based on heat balance calculation.

*4: As discussed in ATHOS analysis report (Ref. 22), the larger number of unit-2 (305 tubes for 2A) is used for the evaluation. Fig.6.2-1 shows the address of the plugged tubes of 2A SG.

Table 6.2-4 Basic parameters for calculation for 3B SG evaluation after plugging

Case	50%	60%	70 %	80 %	90 %	100 %	100 % with no plugging
Plugging[*4]	420	420	420	420	420	420	0
Thermal power (MWt)	869.5 (50%)	1041.4 (60%)	1213.3 (70%)	1385.2 (80%)	1557.1 (90%)	1729 (100%)	1729
RCS flow rate (gpm) [*1]	205,545	205,545	205,545	205,545	205,545	205,545	209,880
T_{hot} (Tsg-in) (°F)							
$T_{sg\text{-}out}$ (°F)[*2]							
T_{cold} (°F)[*2]							
Saturation Steam Pressure (psia)							
Fouling Factor ($ft^2hr°F$ /Btu)							
$T_{feedwater}$ (°F)							
Circulation Ratio							
Steam Mass Flow (lb/hr)							
Feed Water Mass Flow (lb/hr)[*3]							
Blowdown flow rate (gpm)							

Note

*1: Obtained by interpolating the flow rate of 0% plugging and 8% plugging.

*2: RCS flow temperature at SG outlet is assumed to be 0.3°F lower than that at RV inlet. The 0.3°F temperature increase between the SG outlet and RV inlet is caused by heat input from the reactor coolant pump.

*3: Feedwater mass flow rate is the sum of the blowdown flow rate and the steam mass flow based on heat balance calculation.

*4: As discussed in ATHOS analysis report (Ref. 22), the larger number of unit-2 (305 tubes for 2A) is used for the evaluation. Fig.6.2-1 shows the address of the plugged tubes of 2A SG.

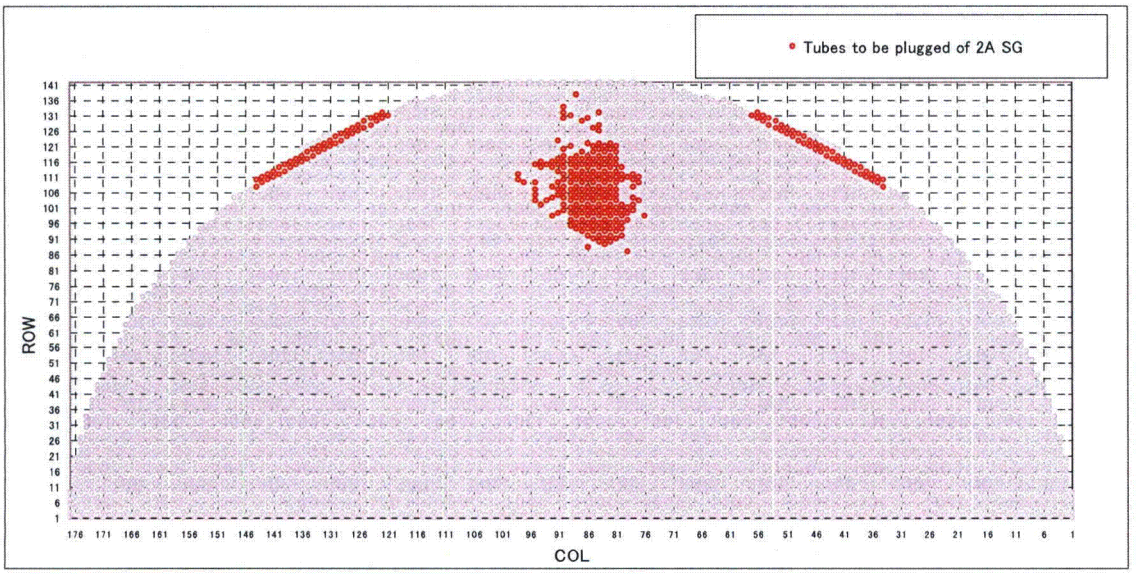

Fig. 6.2-1 Plugging tubes of 2A SG

[ ]

Fig.6.2-2 Tube plugging model of ATHOS for 2A SG

Fig.6.2-3 Flow Characteristics of Row 80 Column 70 (2A SG)

Fig.6.2-4 Flow Characteristics of Row 80 Column 80 (2A SG)

Fig.6.2-5 Flow Characteristics of Row 100 Column 70 (2A SG)

Fig.6.2-6 Flow Characteristics of Row 100 Column 80 (2A SG)

Fig.6.2-7 Flow Characteristics of Row 120 Column 70 (2A SG)

Fig.6.2-8 Flow Characteristics of Row 120 Column 80 (2A SG)

Fig.6.2-9 Flow Characteristics of Row 95 Column 85 (2A SG)

Fig.6.2-10 Flow Characteristics of Row 125 Column 85 (2A SG)

Fig.6.2-11 Flow Characteristics of Row 138 Column 84 (2A SG)

7. Methodology

7.1 Fluid elastic vibration

The term "fluid elastic vibrations" is generally used to refer to self-excited vibration of tube bundles due to cross flow. In 1969, Connors disclosed the presence of this phenomenon for the first time (Ref.23). Fluid-elastic vibration occurs in tube bundles when the amount of energy absorbed by the tubes is greater than the amount that the tubes can dissipate. The measure of the fluid-elastic vibration threshold for any given tube in the bundle (tube stability) is the ratio of the actual velocity of the fluid surrounding the tube to the critical fluid flow velocity for this particular tube. The critical flow velocity Uc required to generate fluid-elastic vibration is obtained using Connor's formula (Ref.23).

$$\frac{U_c}{fD_o} = K\left[\frac{m_0\delta}{\rho_o D_o^{\,2}}\right]^{1/2} \quad \cdots\cdots (3)$$

Where,

U_c	: Critical flow velocity
f	: Tube natural frequency
D_o	: Tube outside diameter
K	: Critical factor
m_0	: Average tube mass per unit length
δ	: Tube logarithmic decrement(= $2\pi h$)
h	: Damping ratio
ρ_o	: Density of water outside the tube

The critical flow velocity U_c in eq. (3) is evaluated in case of tube vibration of single degree of freedom system with uniform cross flow along the tube axis. In actual tube, however, the vibration of the tube supported by the tube support plate is multi degrees of freedom system with beam type of vibration modes. Therefore, considering the vibration mode and fluid distribution, the effective flow velocity U_{en} is evaluated in the following formula.

$$U_{en} = \left[\frac{\int_0^L \frac{\rho(x)}{\rho_0} \cdot U(x)^2 \cdot \phi_n(x)^2 dx}{\int_0^L \frac{m(x)}{m_0} \cdot \phi_n(x)^2 dx} \right]^{1/2} \quad \cdots\cdots(4)$$

Where,

U_{en}	: Nth mode effective flow velocity
$\varphi_n(x)$	: Nth vibration mode
$\rho(x)$	: Fluid density distribution of water outside the tube in tube axis direction
$m(x)$	: Tube mass distribution per unit length in tube axis direction
$U(x)$	: Flow velocity distribution orthogonal to tube axis in tube axis direction
x	: Coordinate component along tube axis
ρ_o	: Average density of water outside the tube
m_o	: Average tube mass per unit length
L	: Tube length

The stability ratio is determined as follows in each vibration mode by calculating the ratio of eq. (3) and eq. (4).

$$SR_n = \frac{U_{en}}{U_{cn}} \quad \cdots\cdots(5)$$

where,

$$\frac{U_{cn}}{f_n \cdot D_o} = K\left[\frac{m_0 \delta}{\rho_o D_o^2}\right]^{1/2} \quad \cdots\cdots(6)$$

This value is called the n-th mode stability ratio SR_n, and if $SR_n > 1$, fluid elastic vibration occurs. Generally, the maximum stability ratio in each mode is called the stability ratio of the tube, which is simply expressed as SR. The uncertainty of SR calculated by the methodology of this section is evaluated in Attachment-6.

7.1.1 Damping ratio and Critical Factor

Although the suggested value by ASME Sec. III Appendix N-1330 for damping ratio is 1.5% and the suggested value for critical factor is 2.4, the values based on recent experimental data are used in this evaluation as follows.

7.1.1.1 Damping ratio

For U-bend tubes in two phase flow, there are four sources of damping: structural damping, two-phase damping, viscous damping and squeeze film damping.

$$\xi = \xi_S + \xi_{TP} + \xi_V + \xi_{SF} \quad \cdots\cdots (7)$$

Where,

ξ_S : Structural damping ratio

ξ_{TP} : Two-phase damping ratio

ξ_V : Viscous damping ratio

ξ_{SF} : Squeeze film damping ratio

(1) Structural damping

The structural damping ratio is estimated with the following experimental equation developed by Pettigrew (Ref.25 and 27). In the case of plugged tubes with Type J stabilizers, the additional damping 0.6% is added

6

$$\xi_S = \left(\frac{N-1}{N}\right)\left[5\left(\frac{L}{\ell_m}\right)^{\frac{1}{2}}\right], \text{ in gas} \cdots\cdots (8)$$

$$\xi_S = \left(\frac{N-1}{N}\right)\left[0.5\left(\frac{L}{\ell_m}\right)^{\frac{1}{2}}\right], \text{ in liquid} \cdots\cdots (9)$$

Where,

ξ_S : Structural damping ratio

N : Number of free spans at U-bend region

N-1 : AVB support points without assuming inactive AVB support points

L : AVB width

l_m : Characteristic tube length: average of the longest three free spans lengths assuming active and/or inactive supports.

This would give:

1 inactive AVB support point (B02):

l_m = 1/3(tube length from TSP #7 hot to B04)

6 inactive AVB support points (B01 to B06):

l_m = 1/3(tube length from TSP #6 hot to B07)

8 inactive AVB support points (B01 to B08):

l_m = 1/3(tube length from TSP #6 hot to B09)

10 inactive AVB support points AVBs (B01 to B10):

l_m = 1/3(tube length from TSP #6 hot to B11)

12 inactive AVB support points AVBs (B01 to B12):

l_m = 1/3(tube length from TSP #6 hot to TSP cold).

(2) Two-phase damping

The two-phase damping depends on the void fraction and fluid properties. Pettigrew's test result of the two phase damping shown in Figure 7.1-2 (Ref.26) is used for this evaluation.

A semi-empirical expression was developed from the experimental data and the functional equation of homogeneous void fraction was obtained as shown in Figure 7.1.2.

The effective homogeneous void fraction is calculated by using the ATHOS outputs and following equation, considering vibration mode.

$$\overline{\beta} = \frac{\int \beta(x)\phi^2 dx}{\int \phi^2 dx} \quad \cdots\cdots(10)$$

Where,

β	: Homogeneous void fraction
Φ	: Vibration mode
x	: Tube axis

The two-phase damping along the tube length is calculated by using Pettigrew's data and the following equation

$$\xi_{TP} = 4\left(\frac{\rho_l D^2}{m_0}\right) f(\beta)\left\{\frac{1+(D/D_e)^3}{\left[1-(D/D_e)^2\right]^2}\right\} \quad \cdots\cdots(11)$$

$$f(\beta) = \begin{cases} \beta/40 & for \quad \beta < 40\% \\ 1 & for \quad 40\% \le \beta \le 70\% \\ 1-(\beta-70)/30 & for \quad \beta > 70\% \end{cases} \quad \cdots\cdots(12)$$

$$D_e = \left(1+\frac{1}{2}P/D_o\right)P \quad \cdots\cdots(13)$$

$$m_0 = m_v + m_p + m_t \quad \cdots\cdots(14)$$

$$m_v = \frac{\pi D_o^2 \rho_o}{4}\left\{\frac{(D_e/D_o)^2+1}{(D_e/D_o)^2-1}\right\} \quad \cdots\cdots(15)$$

Where,

ξ_{TP}	: Two-phase damping
β	: Homogeneous void fraction
D	: Tube outside diameter

P	: Tube pitch
ρ_o	: Density of secondary mixture flow (Calculated by ATHOS)
ρ_l	: Density of secondary liquid flow
m_0	: Average tube mass per unit length
m_v	: Virtual added mass per unit length
m_p	: Mass of primary coolant in tube per unit length
m_t	: Mass of tube metal per unit length

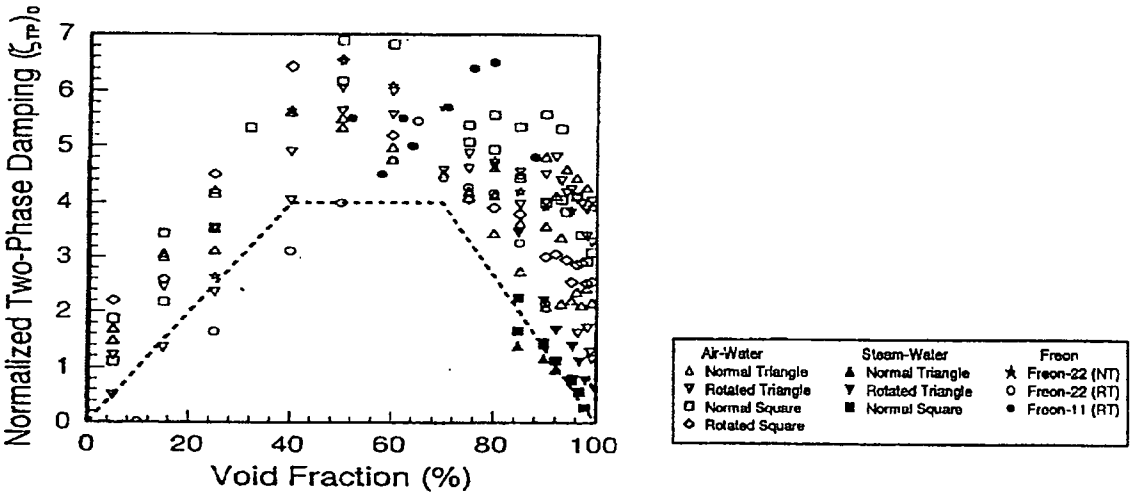

$$(\zeta_{TP})_D = \zeta_{TP}(\rho_\ell D^2/m)^{-1}\{[1+(D/D_c)^3]/[1-(D/D_c)^2]^2\}^{-1}$$

Fig 7.1-2 Effect of void fraction on two-phase damping

(3) Viscous damping

Since the viscous effects are negligibly small in high void fraction (homogeneous void fraction is 40% or greater) (Ref.27), it is not taken into account in this analysis.

(4) Squeeze film damping

Squeeze film damping takes place at the supports and the following equation is based on the available experimental data. (Ref.26)

$$\xi_{SF} = \left(\frac{N-1}{N}\right)\left[\frac{(1460)}{f}\left(\frac{\rho_l D^2}{m_0}\right)\left(\frac{L}{\ell_m}\right)^{\frac{1}{2}}\right] \quad \cdots\cdots(16)$$

Where,

ξ_{SF}	: Squeeze film damping
ρ_l	: Secondary flow liquid density
D	: Tube outside diameter
N	: Number of free spans at U-bend region
N-1	: AVB support points without assuming inactive AVB support points
f	: Natural frequency
L	: AVB width
l_m	: Characteristic tube length
m_0	: Average tube mass per unit length

For unplugged tubes

The support damping (structural and squeeze film) depends on the void fraction. Since the structural damping is increased by a factor of [ ] and the squeeze film damping ratio is zero at the "dry condition", the effect of void fraction is evaluated as follows.

The effect of void fraction at each AVB support point of each tube is taken into consideration. The effective wetness of supports is estimated to determine the damping ratio used for the SR evaluation by the following equations based on the assumptions listed below. (The basis of these assumptions is described in Attachment-2)

- When the void fraction is smaller than [ ] there is a continuous liquid film on the surface of tube. The support is considered "wet," structural damping corresponds to the liquid condition and squeeze film damping is effective.
- When the void fraction is [ ] there is no liquid film on the surface of tube. The support is considered "dry," structural damping corresponds to the gas condition and squeeze film damping is not effective.
- When the void fraction is between [ ] there is a discontinuous liquid film on the surface of tube and the support is considered partially wet. The approach to calculate damping in this void fraction range is described below.

$$N_{WS} = \sum_{i=1}^{N-1} a_i \quad \cdots\cdots (17)$$

$$a_i = \left\{ \left[\quad \right] \right. \quad \cdots\cdots (18)$$

$$N_{DS} = N - 1 - N_{WS} \quad \cdots\cdots (19)$$

Where,

N	: Number of free spans in U-bend
$N-1$	: Number of AVB support points in U-bend
N_{WS}	: Number of effectively wet AVB supports
N_{DS}	: Number of effectively dry AVB supports
i	: AVB support points
α_i	: Void fraction at AVB support points
a_i	: Function of void fraction at AVB support points

By replacing the (N-1/N) term in equations 8 and 9 and combining, structural damping adjusted for void fraction becomes:

[ ] ..... (20)

Similarly replacing the (N-1/N) term in equation 16 with (N_{WS}/N), squeeze film damping adjusted for void fraction becomes:

$$\xi_{SF} = \left(\frac{N_{WS}}{N}\right)\left[\frac{(1460)}{f}\left(\frac{\rho_l D^2}{m_0}\right)\left(\frac{L}{\ell_m}\right)^{\frac{1}{2}}\right] \quad \text{..... (21)}$$

For plugged tubes

The plugged tubes are assumed to be in wet condition despite the void fraction. Equations 7 and 16 are used for structural and squeeze film damping, respectively.

7.1.1.2 Critical Factor

The effect of void fraction, the effect of pitch to diameter ratio, the ratio between In-plane & Out-of-plane and the effect of flow direction are considered to estimate the Connor's constant as follows.

(1) Effect of the void fraction

Based on MHI experimental data (Ref.28), the critical factor K is evaluated using the equation shown in Figure 7.1-3 which indicates the relation between the superficial void fraction and the critical factor. This experiment was performed under two-phase flow condition using the straight tube bundle of the triangular pitch as shown in Table 7.1-1 and Fig.7.1-4.

The effective superficial void fraction along the tube length is calculated by considering vibration mode and using the following equation in the same manner as the two-phase damping. The obtained critical factor obtained is K1, when the value of P/D is 1.33.

$$K_1 = [\quad] \qquad \cdots\cdots(22)$$

$$\overline{\beta} = \frac{\int \beta(x)\phi^2 dx}{\int \phi^2 dx} \qquad \cdots\cdots(23)$$

Where,

β : Homogeneous void fraction

Φ : Vibration mode

x : Tube axis

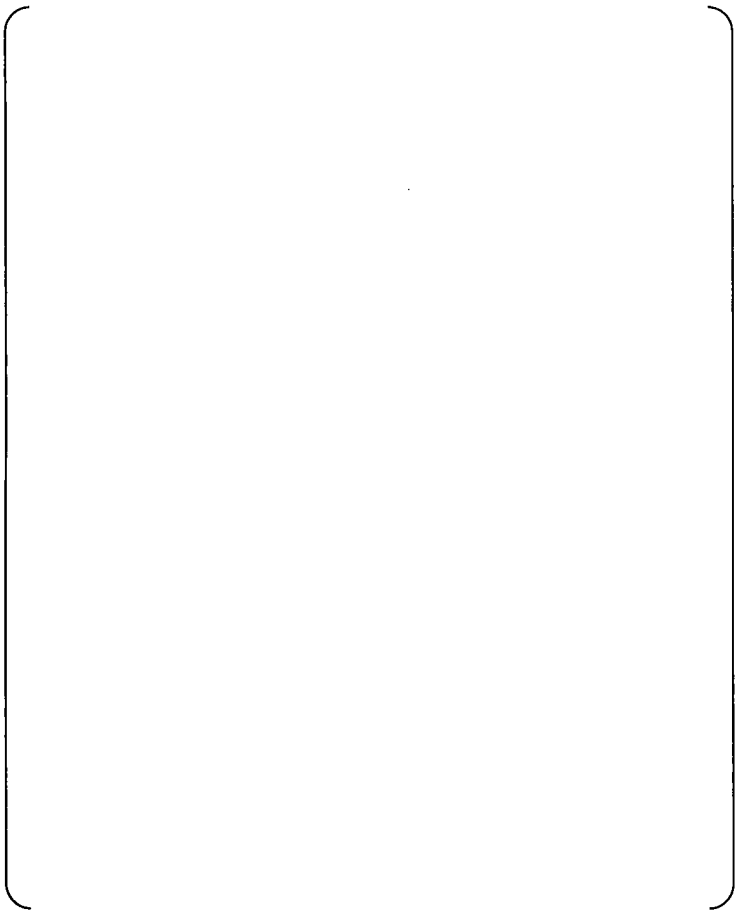

Fig.7.1-3 MHI Experimental Test Result (Relation between Critical Factor and Superficial Void Fraction)

Table 7.1-1 MHI Test Condition

Tube diameter	
Tube pitch	
Number of tubes	
Flow condition	
Pressure	
Temperature	
Superficial void fraction	

Fig.7.1-4 MHI Test Equipment

(2) Effect of P/D

The greater the pitch is, the higher the critical velocity will be. Since the tube bundle has index and the nominal pitch depends on the number of tube Row, the effect of the tube pitch to diameter ratio (P/D) is added to the value obtained in the previous section (K_1). By taking into account of the index of the tube, the effective tube pitch (P_e) is calculated as the average of the triangle sides which includes the tube to be evaluated.

$$P_e = \frac{P_1 + P_2 + P_3}{3} \quad \cdots\cdots(24)$$

Where,

P_e : Effective pitch

P_1, P_2, P_3 : Pithes defined in Fig.7.1-5

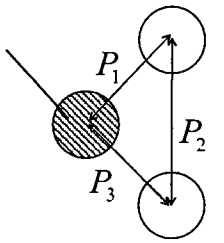

Fig.7.1-5 Effective pitch

The effect of the tube pitch on the Connor's constant is calculated by using the following equation based on Pettigrew's experimental data (Ref.29).

$$K_p = 4.76(P-D)/D + 0.76 \quad \cdots\cdots(25)$$

$$K_o = \frac{K_{p,P/D}}{K_{p,P/D=1.33}} \times K1 \quad \cdots\cdots(26)$$

Where,

K_p : Equation 21

K1 : Critical Factor based on MHI experimental test results by taking into account of the effect of void fraction (P/D=1.33)

$K_{p,P/D}$: Critical Factor based on Pettigrew's experimental test results by taking into account of the effect of P/D

$K_{p,P/D=1.33}$: Critical Factor based on Pettigrew's experimental test results when P/D is 1.33

K_o : Best estimated critical factor of out-of-plane FEI

(3)Critical Factor of In-plane FEI

In accordance with the experiments by T. Nakamura (Ref.30), FEI is observed in the in-plane direction in a single-phase air flow when the tube pitch-to-tube ratio (P/D) is small. The Connor's constant of In-plane FEI is estimated in accordance with the following equation based on Nakamura's experimental data. The ratio between the Connor's constant of in-plane FEI and out-of-plane FEI depends on P/D as shown in Figure 7.1-6. In order to reinforce the basis of Connor's constant used for In-plane FEI evaluation, MHI performed air flow test by using the straight tube bundle of the triangular pitch as shown in Fig. 7.1-7. The ratio of Connor's constant between in-plane and out-of-plane FEI obtained by MHI test result is consistent with Nakamura's experimental data as shown in Fig. 7.1-6. Therefore, the Connor's constant of in-plane FEI for SONGS RSGs is calculated based on the effective tube pitch calculated by taking into account of the index.

$$K_i = \kappa \times K_o \quad \cdots\cdots (27)$$

Where,

κ : Ratio of critical factor of In-plane FEI and out-of-plane FEI

K_i : Best estimated critical factor of In-plane FEI

K_o : Best estimated critical factor of out-of-plane FEI

Ratio κ
Vc(In-flow)/Vc(Out-of-flow)

[ ]

P/D	Fluid	Ratio of critical flow velocity κ =Vc(In-plane) /Vc(Out-of-plane)	Note
1.5	Air-Water	2.7	Violette et al. (2006)
1.37	Air	1.7	Khalvatti et al. (2010)
1.2	Air	0.71	Nakamura et al. (2012)

Fig.7.1-6 Experimental Test Result (Relation between Critical Factor In-plane FEI and P/D)

(a) Test equipment

(b) Test Results

Fig.7.1-7 MHI air flow test

(4) Effect of Flow Direction

The effect of the flow direction on the critical velocity is also determined based on the test result (Ref.31). The greater the angle of the flow direction from the in-plane of tube, the greater the value of the critical velocity will be.

The effect of the flow direction on the critical velocity (increase ratio " a(θ)") is determined based on the test result shown in Fig.7.1-8 (Ref.31). "a(θ)" is defined by the upstream critical flow velocity; not in-plane flow velocity

$$a(\theta) = \frac{U_C(\theta)}{U_C(0\,\mathrm{deg})} \quad \cdots\cdots(28)$$

Where,

θ : Angle of Flow direction

Uc : Critical velocity

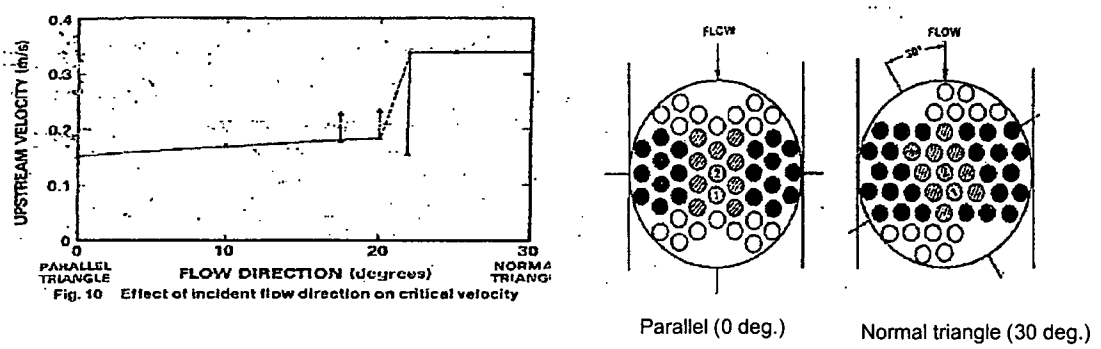

Fig.7.1-8 Effect of the flow direction (Ref.31)

Stability ratio is usually calculated by using in-plane flow velocity V. On the other hand, the function a(θ) is defined by the magnitude of normal flow velocity Vn to the tube. Therefore, K_i or K_o are multiplied by the velocity ratio Vn/V and function a(θ) as shown in Fig.7.1-9, then K used for the analysis is obtained.

$$K = K_i \times Vn/V \times a(\theta) \quad \text{for in-plane FEI evaulation} \cdots\cdots (29)$$

$$K = K_o \times Vn/V \times a(\theta) \quad \text{for out of plane FEI evaluation} \cdots\cdots (30)$$

$$Vn/V = cos\theta \cdots\cdots (31)$$

Where,

a	: Effect of Flow direction
V_n	: Average in-plane velocity
V	: Magnitude of flow velocity
K_i	: Best estimated critical factor of In-plane FEI
K_o	: Best estimated critical factor of out of plane FEI
K	: Best estimated critical factor used for the evaluation

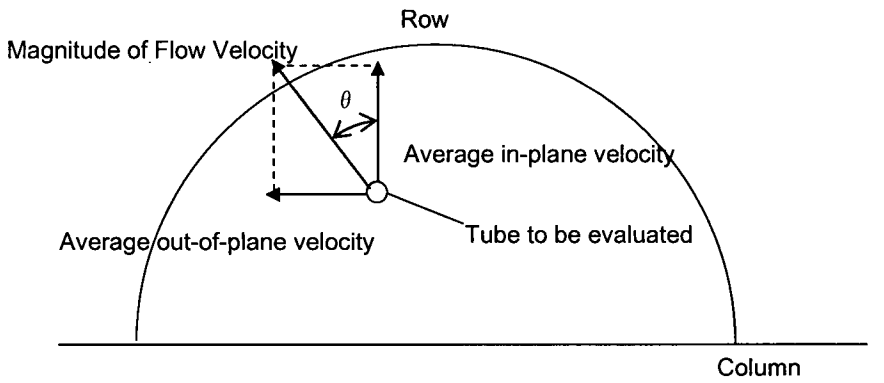

Fig.7.1-9 Effect of flow direction

7.2 Calculation model

Stability analyses are carried out in the following manner.

(1) Tube row

The tubes shown in Table 7.2-1 and Fig.7.2-1 are selected by SCE for the evaluation (see Attachment-7 for details). 6

Table 7.2-1 Evaluated Tubes

Row	Column
80	70
80	80
100	70
100	80
120	70
120	80
95	85
125	85
138	84

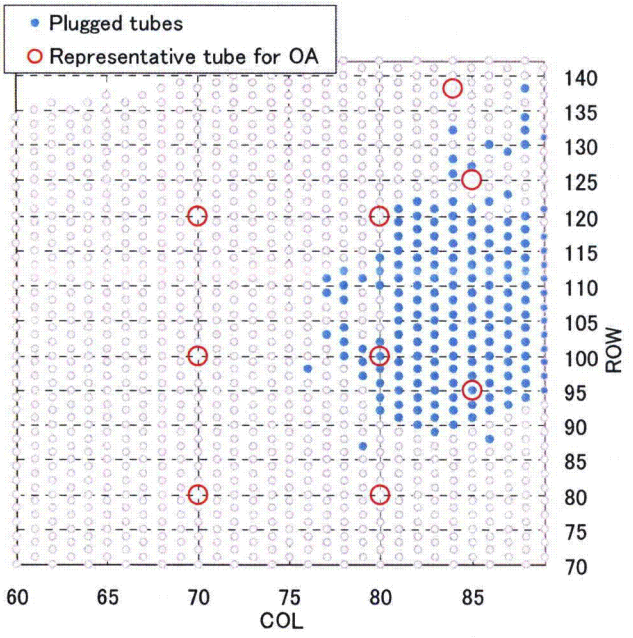

Fig.7.2-1 Evaluated Tubes

(2) Support conditions of AVB (Anti-Vibration Bar) and TSP (Tube Support Plate)

AVB and TSP support points are modeled as pin-supported points. Analysis models including node number and coordinate of TSP elevation are shown in Fig. 7.2-1 to 7.2-9.

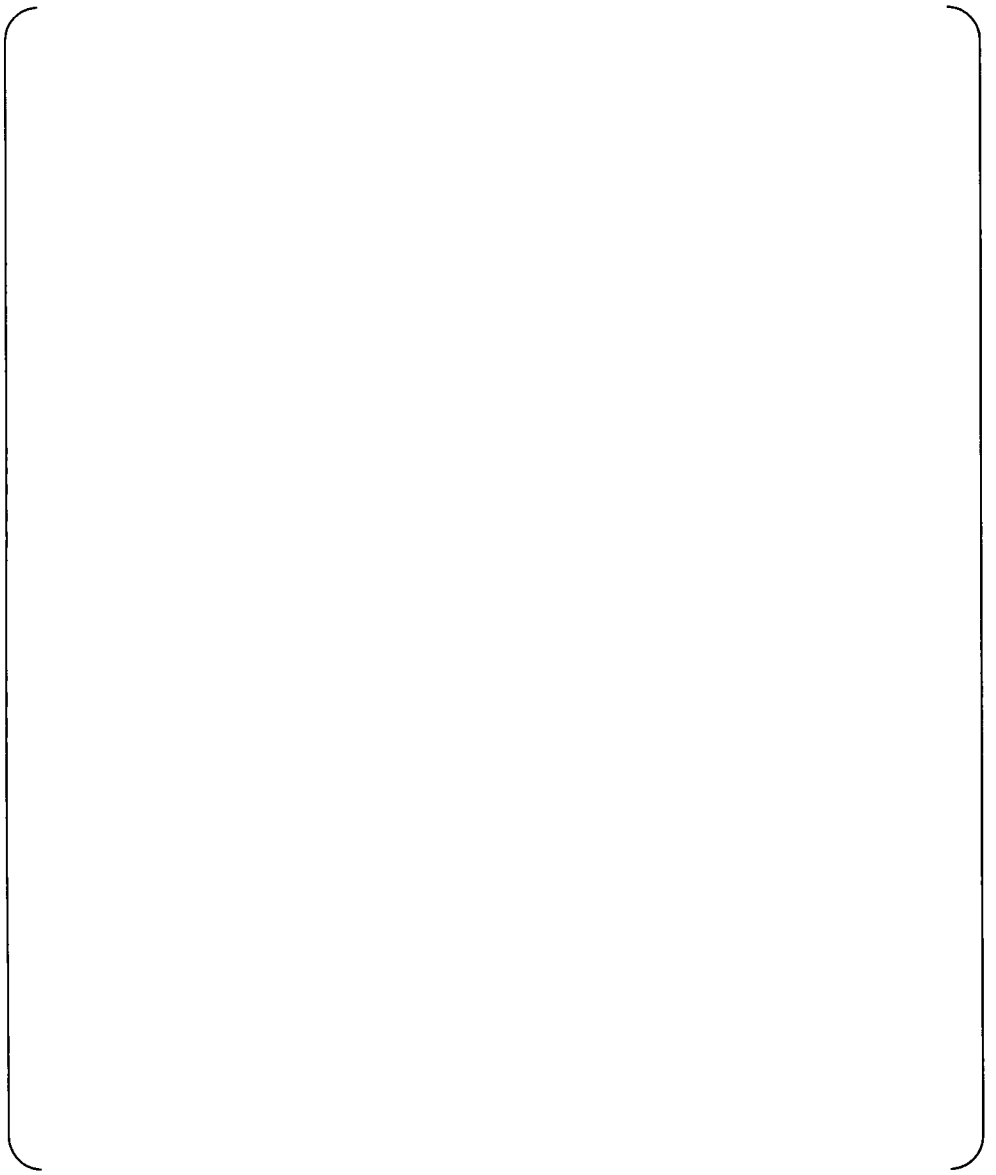

Fig. 7.2-1 Calculation model for Row 80 Column 70

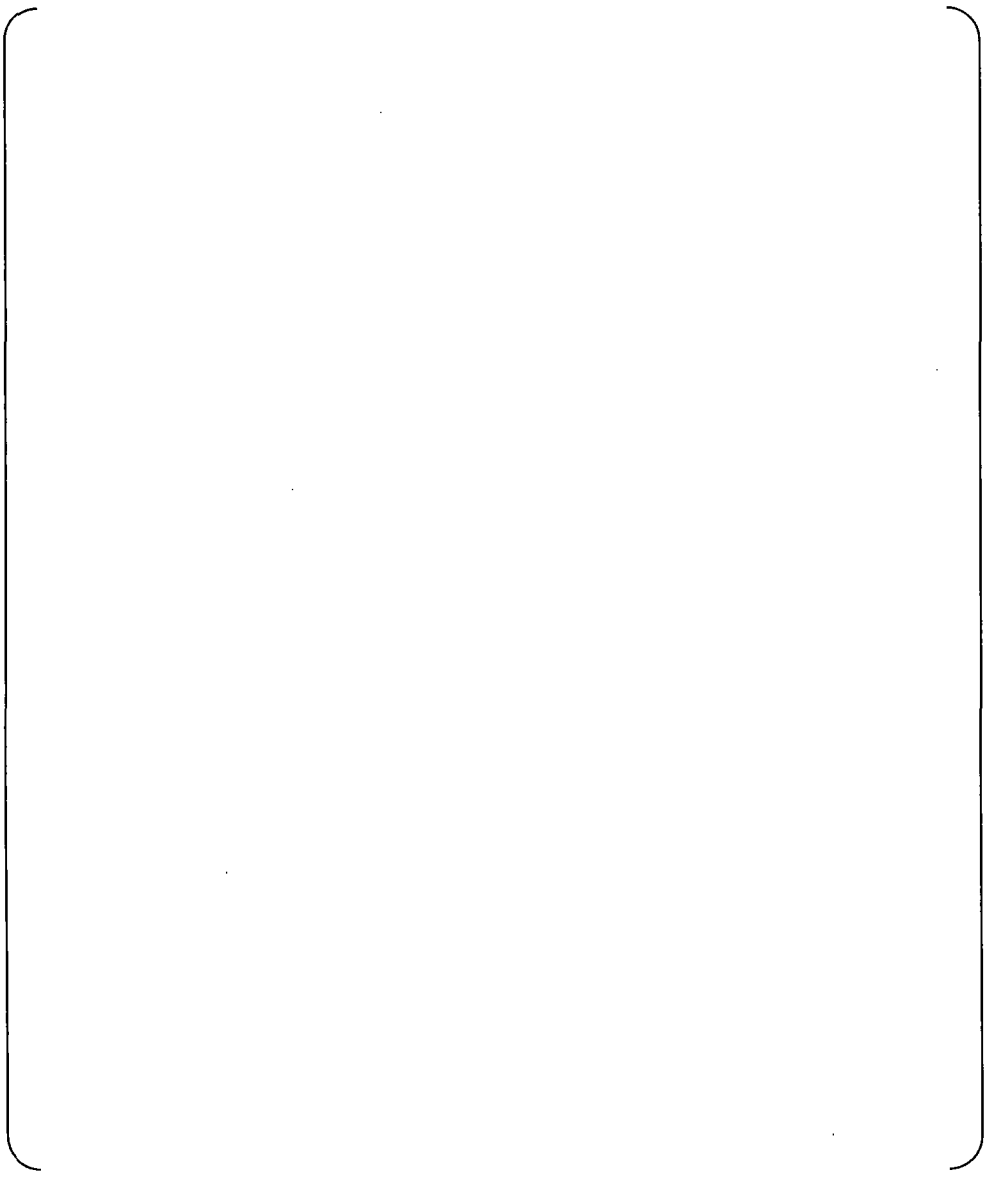

Fig. 7.2-2 Calculation model for Row 80 Column 80

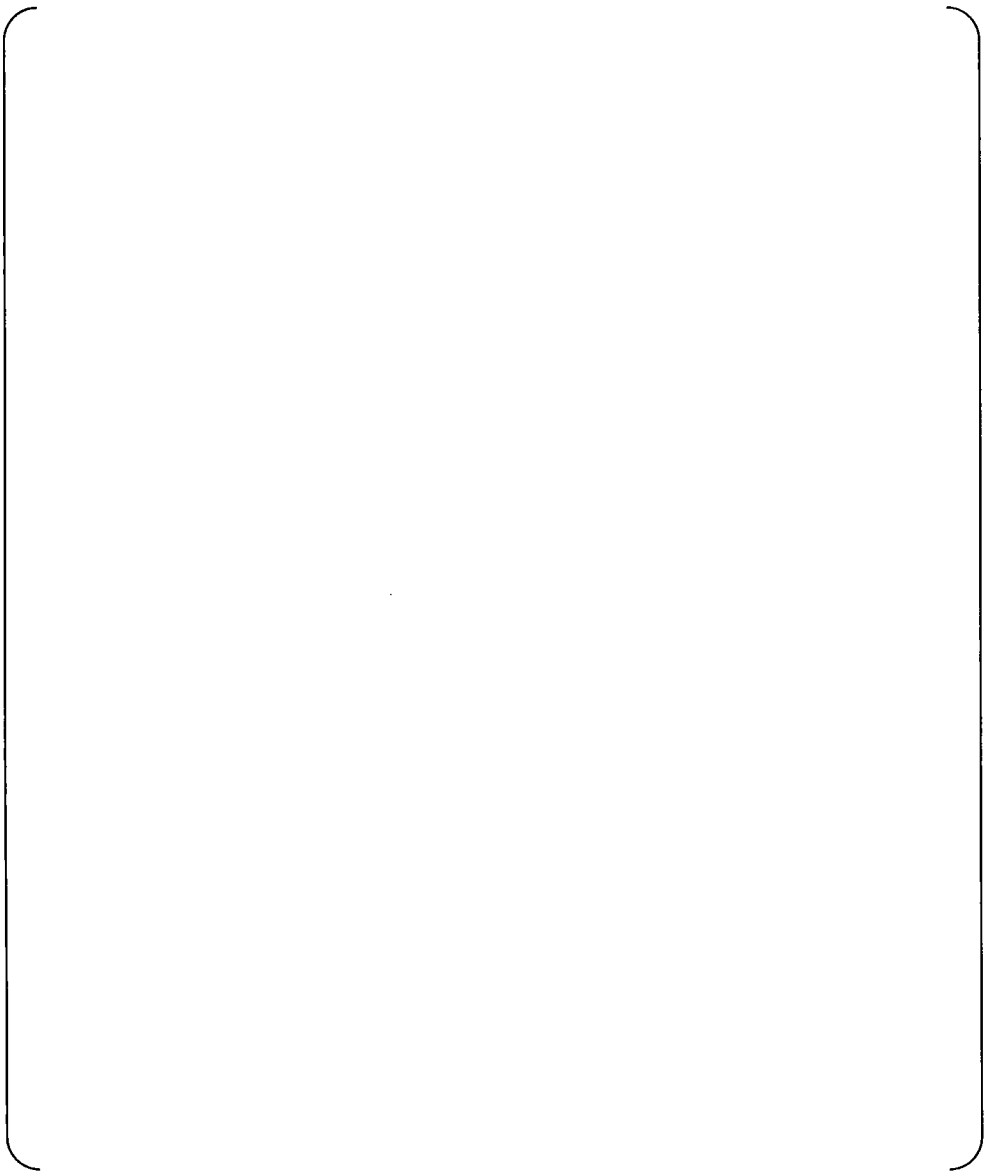

Fig. 7.2-3 Calculation model for Row 100 Column 70

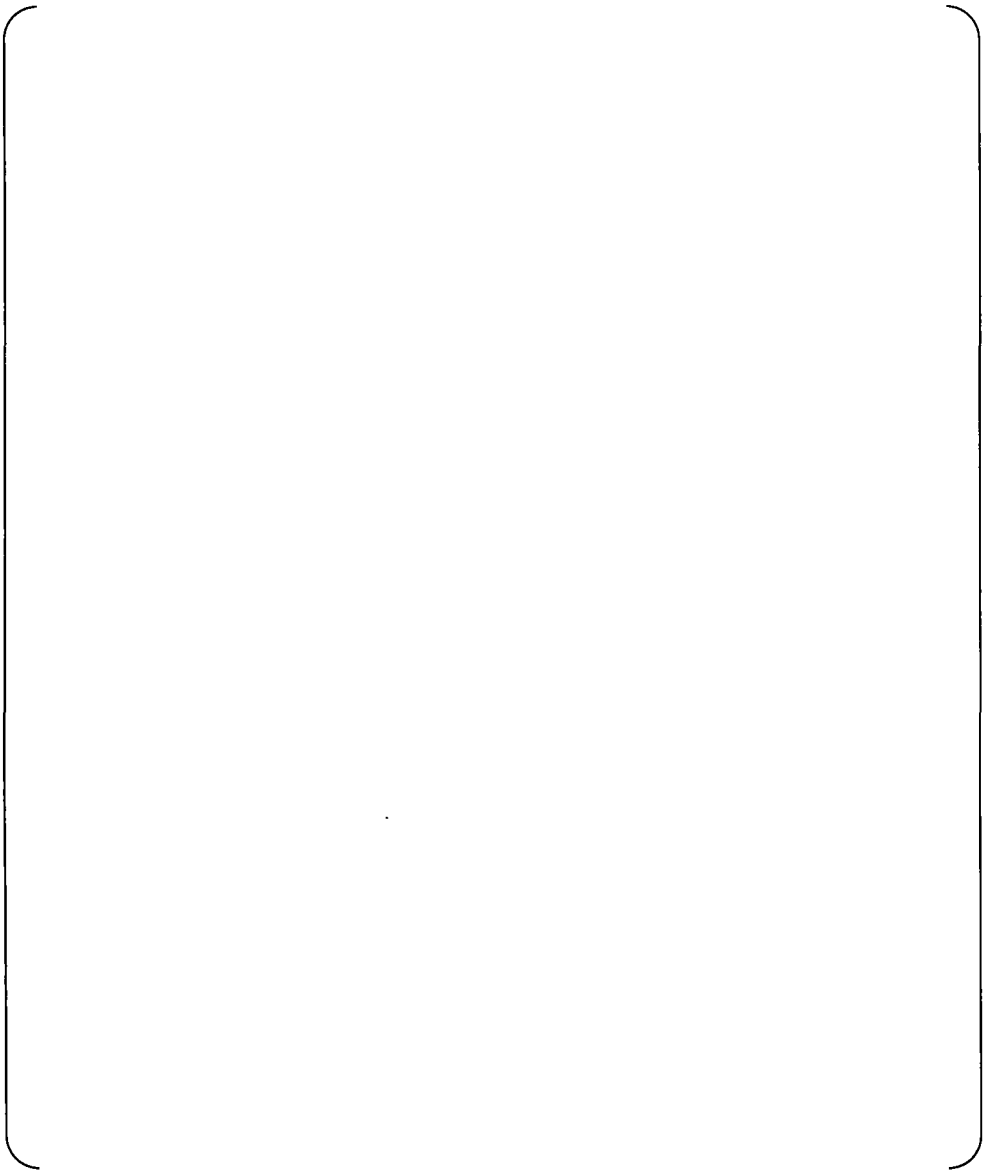

Fig. 7.2-4 Calculation model for Row 100 Column 80

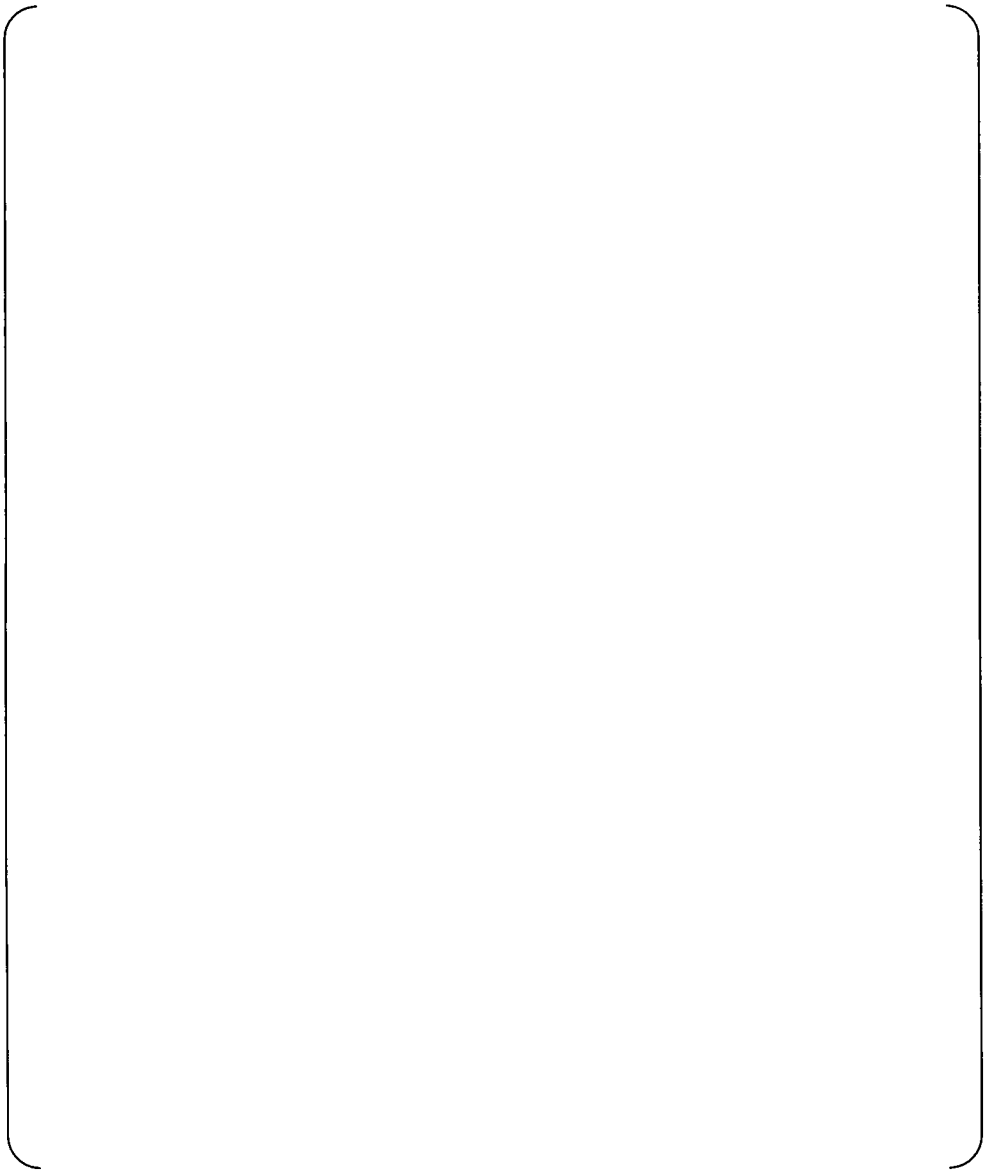

Fig. 7.2-5 Calculation model for Row 120 Column 70

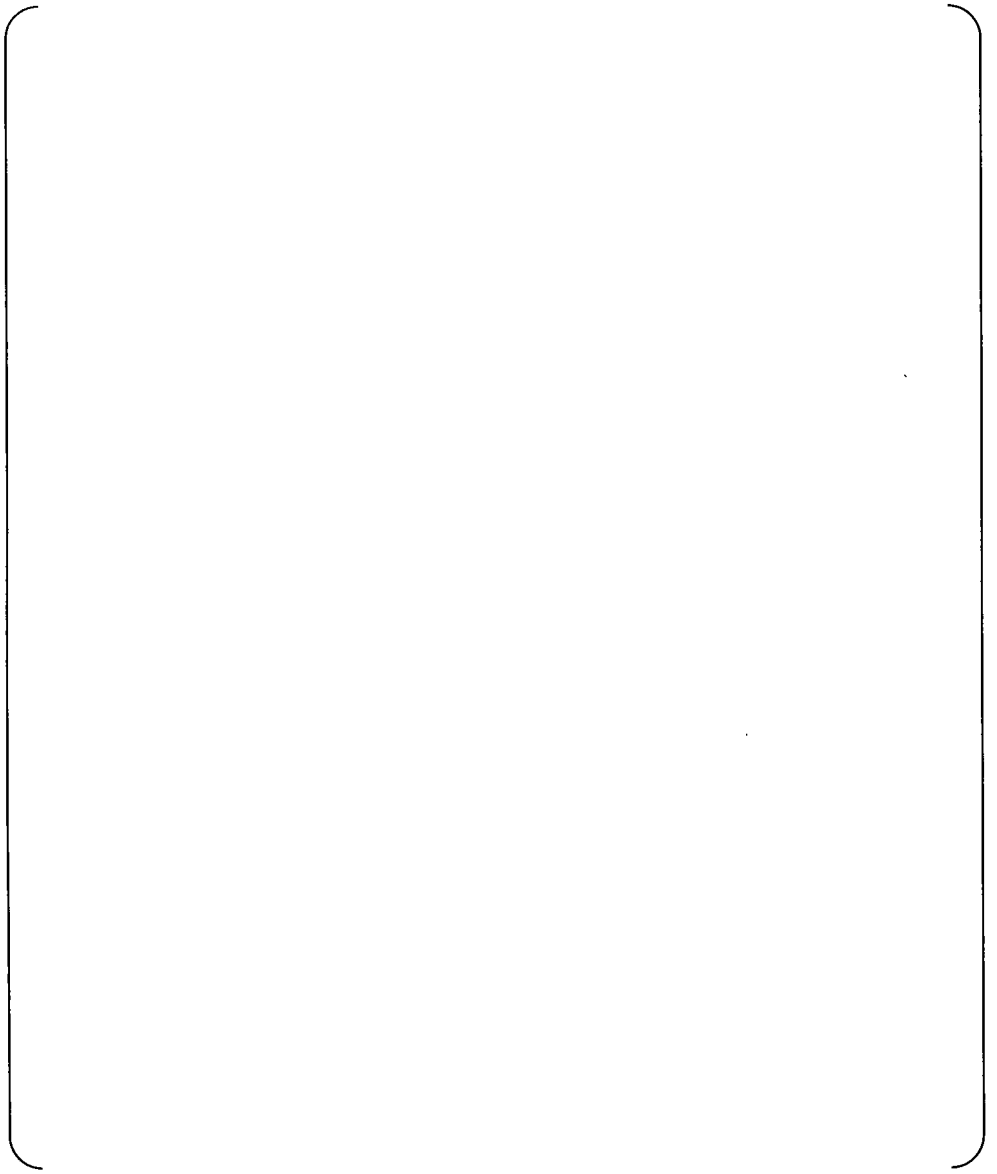

Fig. 7.2-6 Calculation model for Row 120 Column 80

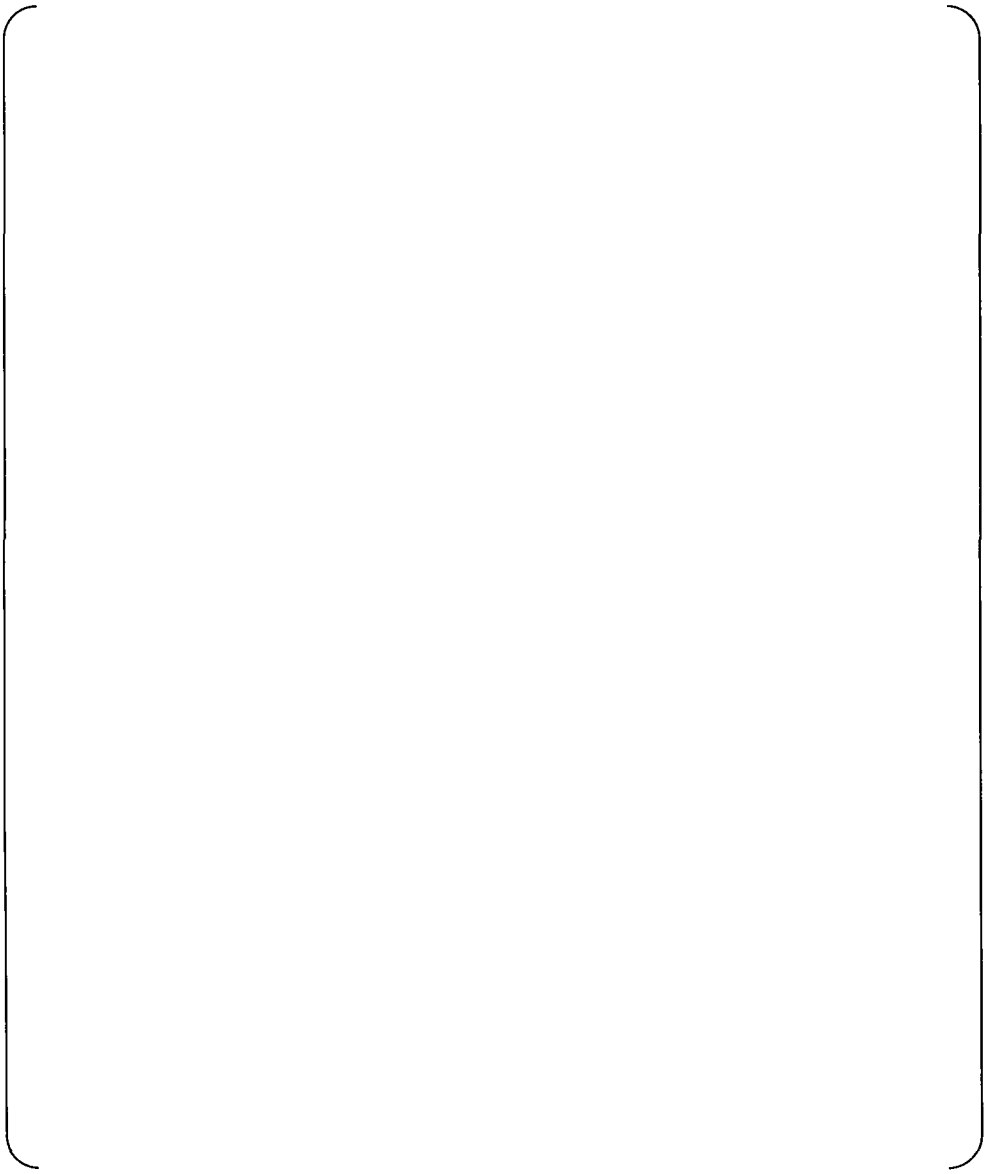

Fig. 7.2-7 Calculation model for Row 95 Column 85

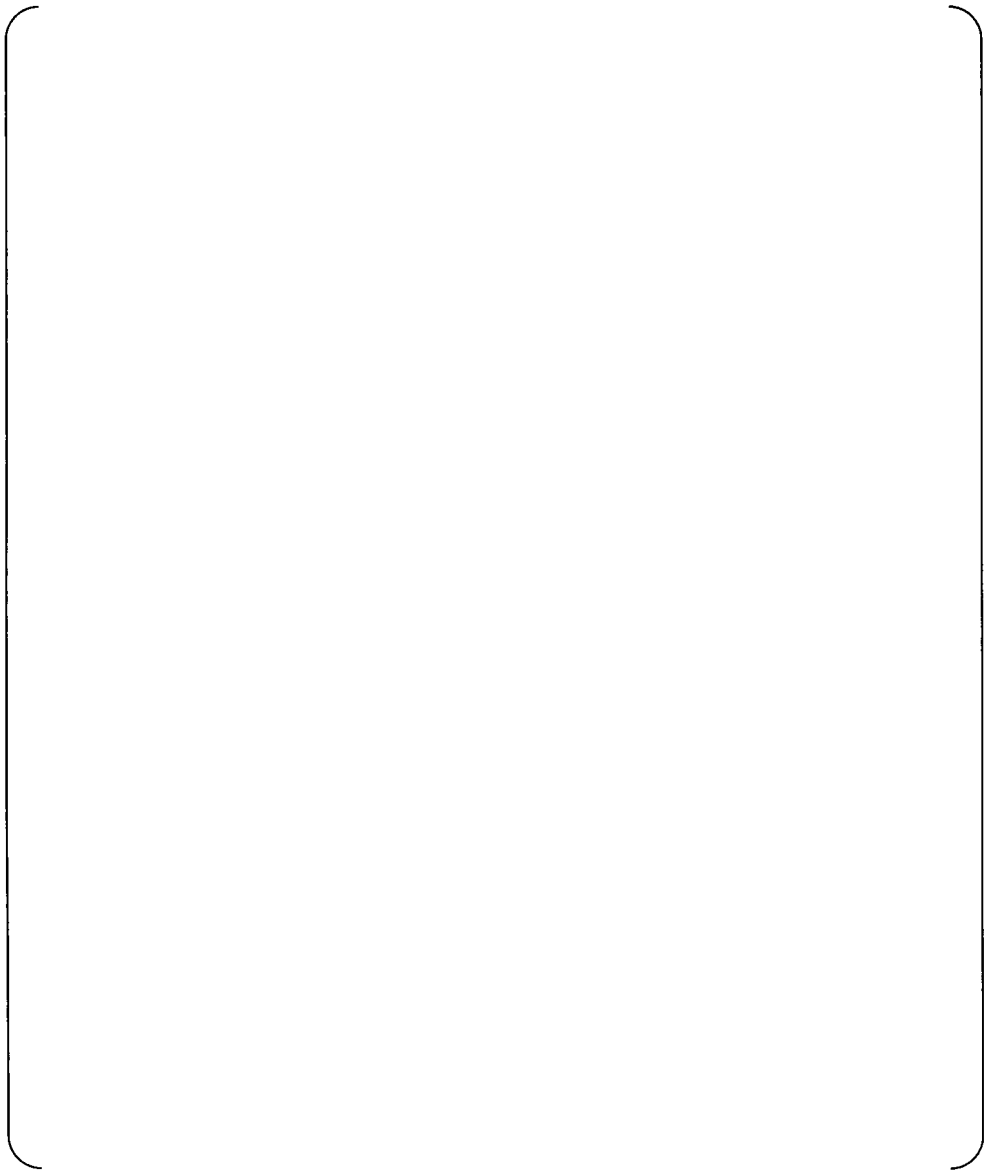

Fig. 7.2-8 Calculation model for Row 125 Column 85

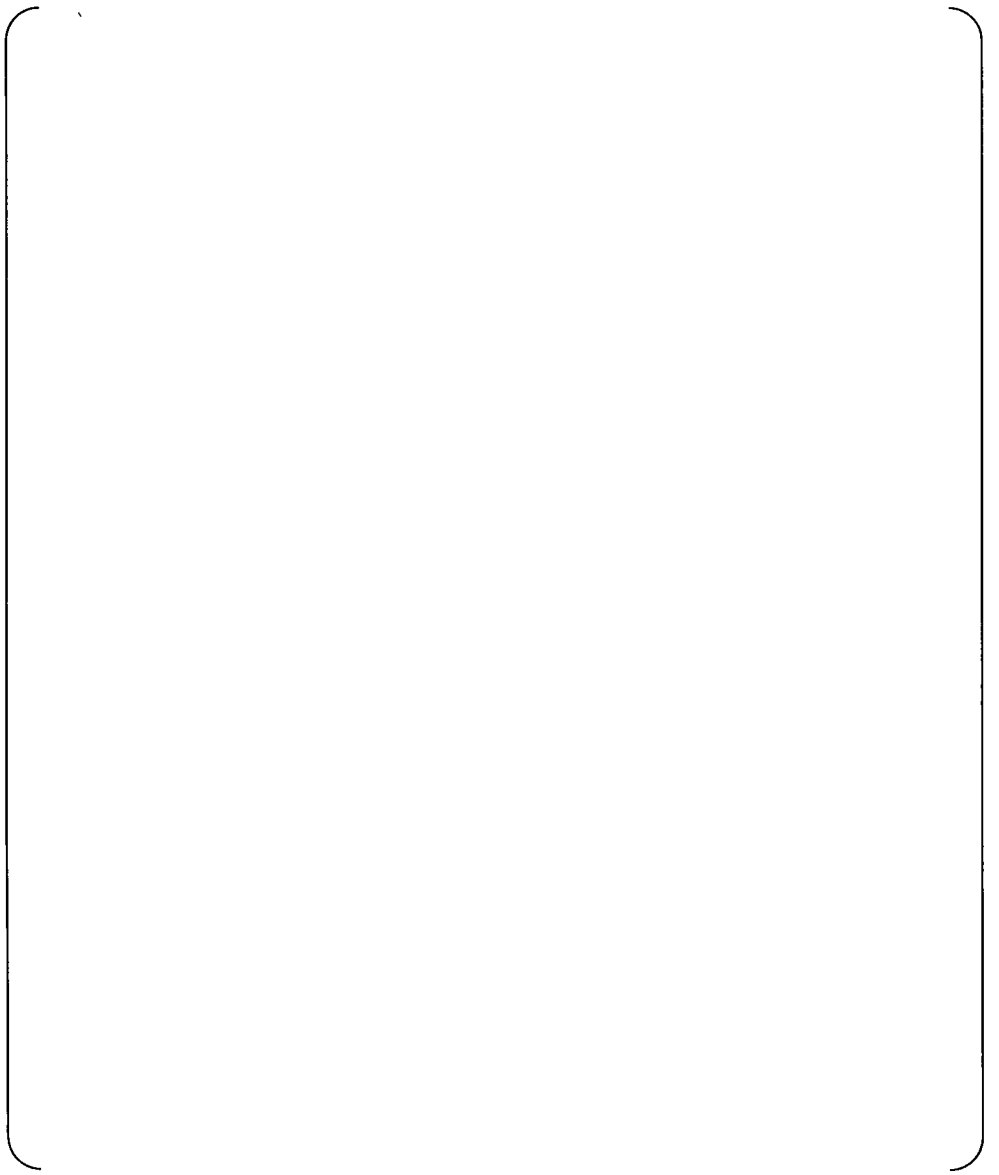

Fig. 7.2-9 Calculation model for Row 138 Column 84

8. Computation Results

8.1 Out of plane FEI analysis results

The out of plane FEI analysis results for 2A SG are shown in Table.8.1.1-1 to 8.1.2-2 as follows.

(1) Assuming all support points active:

For 2A SG

Table 8.1.1-1 All support points are active and the thermal power is 70%

No plugging

Table 8.1.1-2 All support points are active and the thermal power is 100% with no plugging

(2) Assuming 1 support point inactive:

For 2A SG

Table 8.1.2-1 1 support point is inactive and the thermal power is 70%

No plugging

Table 8.1.2-2 1 support point is inactive and the thermal power is 100% with no plugging

Table 8.1.1-1 Out of Plane FEI Analysis Results for 2A SG when the thermal power is 70% and all support points are active

6

Tube		Location of inactive support point	Mode	Tube natural frequency	Damping Ratio h(%)				Critical coefficient				Average fluid density	Average void fraction	Maximum void fraction	Critical flow velocity	Effective flow velocity	Stability ratio
Row	Col			f(Hz)	Structural damping	Two phase damping	Squeeze film damping	Total	K1	K_0	K_θ	K	ρ_0(lb/ft^3)	[-]	[-]	Uc(ft/sec)	Ue(ft/sec)	
80	70	-																
80	80	-																
100	70	-																
100(*)	80(*)	-																
120	70	-																
120	80	-																
95(*)	85(*)	-																
125	85	-																
138	84	-																

Note(*): Plugged tube with Type J stabilizer

Table 8.1.1-2 Out of plane FEI Analysis Results for no plugging model when the thermal power is 100% and all support points are active

6

Tube		Location of inactive support point	Mode	Tube natural frequency	Damping Ratio h(%)				Critical coefficient				Average fluid density	Average void fraction	Maximum void fraction	Critical flow velocity	Effective flow velocity	Stability ratio
Row	Col			f(Hz)	Structural damping	Two phase damping	Squeeze film damping	Total	K1	K_0	K_θ	K	ρ_0(lb/ft^3)	[-]	[-]	Uc(ft/sec)	Ue(ft/sec)	
80	70	-																
80	80	-																
100	70	-																
100	80	-																
120	70	-																
120	80	-																
95	85	-																
125	85	-																
138	84	-																

Table 8.1.2-1 Out of Plane FEI Analysis Results for 2A SG when the thermal power is 70% and 1 support point is inactive

6

Tube		Location of inactive support point	Mode	Tube natural frequency	Damping Ratio h(%)				Critical coefficient				Average fluid density	Average void fraction	Maximum void fraction	Critical flow velocity	Effective flow velocity	Stability ratio
Row	Col			f(Hz)	Structural damping	Two phase damping	Squeeze film damping	Total	K1	K_0	K_θ	K	ρ_0(lb/ft^3)	[-]	[-]	Uc(ft/sec)	Ue(ft/sec)	
80	70	B03																
80	80	B03																
100	70	B03																
100(*)	80(*)	B03																
120	70	B03																
120	80	B03																
95(*)	85(*)	B03																
125	85	B03																
138	84	B04																

Note(*): Plugged tube with Type J stabilizer

Table 8.1.2-2 Out of plane FEI Analysis Results for no plugging model when the thermal power is 100% and 1 support point is inactive

6

Tube		Location of inactive support point	Mode	Tube natural frequency	Damping Ratio h(%)				Critical coefficient				Average fluid density	Average void fraction	Maximum void fraction	Critical flow velocity	Effective flow velocity	Stability ratio
Row	Col			f(Hz)	Structural damping	Two phase damping	Squeeze film damping	Total	K1	K_0	K_θ	K	ρ_0(lb/ft^3)	[-]	[-]	Uc(ft/sec)	Ue(ft/sec)	
80	70	B03																
80	80	B03																
100	70	B02																
100	80	B02																
120	70	B02																
120	80	B02																
95	85	B03																
125	85	B02																
138	84	B02																

8.2 In-plane FEI analysis results

The in-plane FEI analysis results are shown in Table 8.2.1-1 to 8.2.4-7 as follows.

(1) Assuming 6 support points are inactive:

For 2A SG

Table 8.2.1-1 6 consecutive support points are inactive and the thermal power is 50%

Table 8.2.1-2 6 consecutive support points are inactive and the thermal power is 60%

Table 8.2.1-3 6 consecutive support points are inactive and the thermal power is 70%

Table 8.2.1-4 6 consecutive support points are inactive and the thermal power is 80%

Table 8.2.1-5 6 consecutive support points are inactive and the thermal power is 90%

Table 8.2.1-6 6 consecutive support points are inactive and the thermal power is 100%

No plugging

Table 8.2.1-7 6 consecutive support points are inactive and the thermal power is 100% with no plugging

(2) Assuming 8 support points are inactive:

For 2A SG

Table 8.2.2-1 8 consecutive support points are inactive and the thermal power is 50%

Table 8.2.2-2 8 consecutive support points are inactive and the thermal power is 60%

Table 8.2.2-3 8 consecutive support points are inactive and the thermal power is 70%

Table 8.2.2-4 8 consecutive support points are inactive and the thermal power is 80%

Table 8.2.2-5 8 consecutive support points are inactive and the thermal power is 90%

Table 8.2.2-6 8 consecutive support points are inactive and the thermal power is 100%

No plugging

Table 8.2.2-7 8 consecutive support points are inactive and the thermal power is 100% with no plugging

(3) Assuming 10 support points are inactive:

For 2A SG

Table 8.2.3-1 10 consecutive support points are inactive and the thermal power is 50%

Table 8.2.3-2 10 consecutive support points are inactive and the thermal power is 60%

Table 8.2.3-3 10 consecutive support points are inactive and the thermal power is 70%

Table 8.2.3-4 10 consecutive support points are inactive and the thermal power is 80%

Table 8.2.3-5 10 consecutive support points are inactive and the thermal power is 90%

Table 8.2.3-6 10 consecutive support points are inactive and the thermal power is 100%

No plugging

Table 8.2.3-7 10 consecutive support points are inactive and the thermal power is 100% with no plugging

(4) Assuming All support points are inactive:

For 2A SG

Table 8.2.4-1 All consecutive support points are inactive and the thermal power is 50%

Table 8.2.4-2 All consecutive support points are inactive and the thermal power is 60%

Table 8.2.4-3 All consecutive support points are inactive and the thermal power is 70%

Table 8.2.4-4 All consecutive support points are inactive and the thermal power is 80%

Table 8.2.4-5 All consecutive support points are inactive and the thermal power is 90%

Table 8.2.4-6 All consecutive support points are inactive and the thermal power is 100%

No plugging

Table 8.2.4-7 All consecutive support points are inactive and the thermal power is 100% with no plugging

Table 8.2.1-1 In-plane FEI Analysis Results for 2A SG when the thermal power is 50% and 6 consecutive support points are inactive

Tube		Mode	Tube natural frequency	Damping Ratio h(%)				Critical coefficient					Average fluid density	Average void fraction	Maximum void fraction	Critical flow velocity	Effective flow velocity	Stability ratio
Row	Col		f(Hz)	Structural damping	Two phase damping	Squeeze film damping	Total	K1	K_0	K_i	K_θ	K	ρ_0(lb/ft^3)	[-]	[-]	Uc(ft/sec)	Ue(ft/sec)	
80	70																	
80	80																	
100	70																	
100(*)	80(*)																	
120	70																	
120	80																	
95(*)	85(*)																	
125	85																	
138	84																	

Note(*): Plugged tube with Type J stabilizer

Table 8.2.1-2 In-plane FEI Analysis Results for 2A SG when the thermal power is 60% and 6 consecutive support points are inactive

Tube		Mode	Tube natural frequency	Damping Ratio h(%)				Critical coefficient					Average fluid density	Average void fraction	Maximum void fraction	Critical flow velocity	Effective flow velocity	Stability ratio
Row	Col		f(Hz)	Structural damping	Two phase damping	Squeeze film damping	Total	K1	K_0	K_i	K_θ	K	ρ_0(lb/ft^3)	[-]	[-]	Uc(ft/sec)	Ue(ft/sec)	
80	70																	
80	80																	
100	70																	
100(*)	80(*)																	
120	70																	
120	80																	
95(*)	85(*)																	
125	85																	
138	84																	

Note(*): Plugged tube with Type J stabilizer

6

6

6

Non-proprietary Version

Document No.L5-04GA567(6)

(68/149)

MITSUBISHI HEAVY INDUSTRIES, LTD.

Table 8.2.1-3 In-plane FEI Analysis Results for 2A SG when the thermal power is 70% and 6 consecutive support points are inactive

Tube		Mode	Tube natural frequency	Damping Ratio h(%)				Critical coefficient					Average fluid density	Average void fraction	Maximum void fraction	Critical flow velocity	Effective flow velocity	Stability ratio
Row	Col		f(Hz)	Structural damping	Two phase damping	Squeeze film damping	Total	K1	K_0	K_i	K_θ	K	ρ_0(lb/ft^3)	[-]	[-]	Uc(ft/sec)	Ue(ft/sec)	
80	70																	
80	80																	
100	70																	
100(*)	80(*)																	
120	70																	
120	80																	
95(*)	85(*)																	
125	85																	
138	84																	

Note(*): Plugged tube with Type J stabilizer

△6 △6 △6

Non-proprietary Version

Document No.L5-04GA567(6)

(69/149)

MITSUBISHI HEAVY INDUSTRIES, LTD.

Table 8.2.1-4 In-plane FEI Analysis Results for 2A SG when the thermal power is 80% and 6 consecutive support points are inactive

Tube		Mode	Tube natural frequency	Damping Ratio h(%)				Critical coefficient					Average fluid density	Average void fraction	Maximum void fraction	Critical flow velocity	Effective flow velocity	Stability ratio
Row	Col		f(Hz)	Structural damping	Two phase damping	Squeeze film damping	Total	K1	K_0	K_i	K_θ	K	ρ_0(lb/ft^3)	[-]	[-]	Uc(ft/sec)	Ue(ft/sec)	
80	70																	
80	80																	
100	70																	
100(*)	80(*)																	
120	70																	
120	80																	
95(*)	85(*)																	
125	85																	
138	84																	

Note(*): Plugged tube with Type J stabilizer

6

6

6

Table 8.2.1-5 In-plane FEI Analysis Results for 2A SG when the thermal power is 90% and 6 consecutive support points are inactive

Tube		Mode	Tube natural frequency	Damping Ratio h(%)				Critical coefficient					Average fluid density	Average void fraction	Maximum void fraction	Critical flow velocity	Effective flow velocity	Stability ratio
Row	Col		f(Hz)	Structural damping	Two phase damping	Squeeze film damping	Total	K1	K_0	K_i	K_θ	K	ρ_0(lb/ft^3)	[-]	[-]	Uc(ft/sec)	Ue(ft/sec)	
80	70																	
80	80																	
100	70																	
100(*)	80(*)																	
120	70																	
120	80																	
95(*)	85(*)																	
125	85																	
138	84																	

Note(*): Plugged tube with Type J stabilizer

△6 △6 △6

Non-proprietary Version

Document No.L5-04GA567(6) (71/149)

MITSUBISHI HEAVY INDUSTRIES, LTD.

Table 8.2.1-6 In-plane FEI Analysis Results for 2A SG when the thermal power is 100% and 6 consecutive support points are inactive

Tube		Mode	Tube natural frequency	Damping Ratio h(%)				Critical coefficient					Average fluid density	Average void fraction	Maximum void fraction	Critical flow velocity	Effective flow velocity	Stability ratio
Row	Col		f(Hz)	Structural damping	Two phase damping	Squeeze film damping	Total	K1	K_0	K_i	K_θ	K	ρ_0(lb/ft^3)	[-]	[-]	Uc(ft/sec)	Ue(ft/sec)	
80	70																	
80	80																	
100	70																	
100(*)	80(*)																	
120	70																	
120	80																	
95(*)	85(*)																	
125	85																	
138	84																	

Note(*): Plugged tube with Type J stabilizer

6 6 6

Non-proprietary Version

Document No.L5-04GA567(6)

(72/149)

MITSUBISHI HEAVY INDUSTRIES, LTD.

Table 8.2.1-7 In-plane FEI Analysis Results for no plugging model when the thermal power is 100% and 6 consecutive support points are inactive

Tube		Mode	Tube natural frequency	Damping Ratio h(%)				Critical coefficient					Average fluid density	Average void fraction	Maximum void fraction	Critical flow velocity	Effective flow velocity	Stability ratio
Row	Col		f(Hz)	Structural damping	Two phase damping	Squeeze film damping	Total	K1	K_0	K_i	K_θ	K	ρ_0(lb/ft^3)	[-]	[-]	Uc(ft/sec)	Ue(ft/sec)	
80	70																	
80	80																	
100	70																	
100	80																	
120	70																	
120	80																	
95	85																	
125	85																	
138	84																	

Table 8.2.2-1 In-plane FEI Analysis Results for 2A SG when the thermal power is 50% and 8 consecutive support points are inactive

Tube		Mode	Tube natural frequency	Damping Ratio h(%)				Critical coefficient					Average fluid density	Average void fraction	Maximum void fraction	Critical flow velocity	Effective flow velocity	Stability ratio
Row	Col		f(Hz)	Structural damping	Two phase damping	Squeeze film damping	Total	K1	K_0	K_i	K_θ	K	ρ_0(lb/ft^3)	[-]	[-]	Uc(ft/sec)	Ue(ft/sec)	
80	70																	
80	80																	
100	70																	
100(*)	80(*)																	
120	70																	
120	80																	
95(*)	85(*)																	
125	85																	
138	84																	

Note(*): Plugged tube with Type J stabilizer

6 6 6

Non-proprietary Version

Document No.L5-04GA567(6)

Table 8.2.2-2 In-plane FEI Analysis Results for 2A SG when the thermal power is 60% and 8 consecutive support points are inactive

Tube		Mode	Tube natural frequency	Damping Ratio h(%)				Critical coefficient					Average fluid density	Average void fraction	Maximum void fraction	Critical flow velocity	Effective flow velocity	Stability ratio
Row	Col		f(Hz)	Structural damping	Two phase damping	Squeeze film damping	Total	K1	K_0	K_i	K_θ	K	ρ_0(lb/ft^3)	[-]	[-]	Uc(ft/sec)	Ue(ft/sec)	
80	70																	
80	80																	
100	70																	
100(*)	80(*)																	
120	70																	
120	80																	
95(*)	85(*)																	
125	85																	
138	84																	

Note(*): Plugged tube with Type J stabilizer

6 6 6

Non-proprietary Version

Document No.L5-04GA567(6)

(75/149)

MITSUBISHI HEAVY INDUSTRIES, LTD.

Table 8.2.2-3 In-plane FEI Analysis Results for 2A SG when the thermal power is 70% and 8 consecutive support points are inactive

Tube		Mode	Tube natural frequency	Damping Ratio h(%)				Critical coefficient					Average fluid density	Average void fraction	Maximum void fraction	Critical flow velocity	Effective flow velocity	Stability ratio
Row	Col		f(Hz)	Structural damping	Two phase damping	Squeeze film damping	Total	K1	K_0	K_i	K_θ	K	ρ_0(lb/ft^3)	[-]	[-]	Uc(ft/sec)	Ue(ft/sec)	
80	70																	
80	80																	
100	70																	
100(*)	80(*)																	
120	70																	
120	80																	
95(*)	85(*)																	
125	85																	
138	84																	

Note(*): Plugged tube with Type J stabilizer

6 6 6

Non-proprietary Version

Document No.L5-04GA567(6)

(76/149)

MITSUBISHI HEAVY INDUSTRIES, LTD.

Table 8.2.2-4 In-plane FEI Analysis Results for 2A SG when the thermal power is 80% and 8 consecutive support points are inactive

Tube		Mode	Tube natural frequency	Damping Ratio h(%)				Critical coefficient					Average fluid density	Average void fraction	Maximum void fraction	Critical flow velocity	Effective flow velocity	Stability ratio
Row	Col		f(Hz)	Structural damping	Two phase damping	Squeeze film damping	Total	K1	K_0	K_i	K_θ	K	ρ_0(lb/ft^3)	[-]	[-]	Uc(ft/sec)	Ue(ft/sec)	
80	70																	
80	80																	
100	70																	
100(*)	80(*)																	
120	70																	
120	80																	
95(*)	85(*)																	
125	85																	
138	84																	

Note(*): Plugged tube with Type J stabilizer

6

6

6

Table 8.2.2-5 In-plane FEI Analysis Results for 2A SG when the thermal power is 90% and 8 consecutive support points are inactive

Tube		Mode	Tube natural frequency	Damping Ratio h(%)				Critical coefficient					Average fluid density	Average void fraction	Maximum void fraction	Critical flow velocity	Effective flow velocity	Stability ratio
Row	Col		f(Hz)	Structural damping	Two phase damping	Squeeze film damping	Total	K1	K_0	K_i	K_θ	K	ρ_0(lb/ft^3)	[-]	[-]	Uc(ft/sec)	Ue(ft/sec)	
80	70																	
80	80																	
100	70																	
100(*)	80(*)																	
120	70																	
120	80																	
95(*)	85(*)																	
125	85																	
138	84																	

Note(*): Plugged tube with Type J stabilizer

6 6 6

Non-proprietary Version

Document No.L5-04GA567(6)

(78/149)

MITSUBISHI HEAVY INDUSTRIES, LTD.

Table 8.2.2-6 In-plane FEI Analysis Results for 2A SG when the thermal power is 100% and 8 consecutive support points are inactive

Tube		Mode	Tube natural frequency	Damping Ratio h(%)				Critical coefficient					Average fluid density	Average void fraction	Maximum void fraction	Critical flow velocity	Effective flow velocity	Stability ratio
Row	Col		f(Hz)	Structural damping	Two phase damping	Squeeze film damping	Total	K1	K_0	K_i	K_θ	K	ρ_0(lb/ft^3)	[-]	[-]	Uc(ft/sec)	Ue(ft/sec)	
80	70																	
80	80																	
100	70																	
100(*)	80(*)																	
120	70																	
120	80																	
95(*)	85(*)																	
125	85																	
138	84																	

Note(*): Plugged tube with Type J stabilizer

6 6 6

Non-proprietary Version

Document No.L5-04GA567(6)

Table 8.2.2-7 In-plane FEI Analysis Results for no plugging model when the thermal power is 100% and 8 consecutive support points are inactive

Tube		Mode	Tube natural frequency	Damping Ratio h(%)				Critical coefficient					Average fluid density	Average void fraction	Maximum void fraction	Critical flow velocity	Effective flow velocity	Stability ratio
Row	Col		f(Hz)	Structural damping	Two phase damping	Squeeze film damping	Total	K1	K_0	K_i	K_θ	K	ρ_0(lb/ft^3)	[-]	[-]	Uc(ft/sec)	Ue(ft/sec)	
80	70																	
80	80																	
100	70																	
100	80																	
120	70																	
120	80																	
95	85																	
125	85																	
138	84																	

Table 8.2.3-1 In-plane FEI Analysis Results for 2A SG when the thermal power is 50% and 10 consecutive support points are inactive

Tube		Mode	Tube natural frequency	Damping Ratio h(%)				Critical coefficient					Average fluid density	Average void fraction	Maximum void fraction	Critical flow velocity	Effective flow velocity	Stability ratio
Row	Col		f(Hz)	Structural damping	Two phase damping	Squeeze film damping	Total	K1	K_0	K_i	K_θ	K	ρ_0(lb/ft^3)	[-]	[-]	Uc(ft/sec)	Ue(ft/sec)	
80	70																	
80	80																	
100	70																	
100(*)	80(*)																	
120	70																	
120	80																	
95(*)	85(*)																	
125	85																	
138	84																	

Note(*): Plugged tube with Type J stabilizer

6

6

6

Non-proprietary Version

Document No.L5-04GA567(6)

(81/149)

MITSUBISHI HEAVY INDUSTRIES, LTD.

Table 8.2.3-2 In-plane FEI Analysis Results for 2A SG when the thermal power is 60% and 10 consecutive support points are inactive

Tube		Mode	Tube natural frequency	Damping Ratio h(%)				Critical coefficient					Average fluid density	Average void fraction	Maximum void fraction	Critical flow velocity	Effective flow velocity	Stability ratio
Row	Col		f(Hz)	Structural damping	Two phase damping	Squeeze film damping	Total	K1	K_0	K_i	K_θ	K	ρ_0(lb/ft^3)	[-]	[-]	Uc(ft/sec)	Ue(ft/sec)	
80	70																	
80	80																	
100	70																	
100(*)	80(*)																	
120	70																	
120	80																	
95(*)	85(*)																	
125	85																	
138	84																	

Note(*): Plugged tube with Type J stabilizer

6 6 6

Non-proprietary Version

Document No.L5-04GA567(6)

(82/149)

MITSUBISHI HEAVY INDUSTRIES, LTD.

Table 8.2.3-3 In-plane FEI Analysis Results for 2A SG when the thermal power is 70% and 10 consecutive support points are inactive

Tube		Mode	Tube natural frequency	Damping Ratio h(%)				Critical coefficient					Average fluid density	Average void fraction	Maximum void fraction	Critical flow velocity	Effective flow velocity	Stability ratio
Row	Col		f(Hz)	Structural damping	Two phase damping	Squeeze film damping	Total	K1	K_0	K_i	K_θ	K	ρ_0(lb/ft^3)	[-]	[-]	Uc(ft/sec)	Ue(ft/sec)	
80	70																	
80	80																	
100	70																	
100(*)	80(*)																	
120	70																	
120	80																	
95(*)	85(*)																	
125	85																	
138	84																	

Note(*): Plugged tube with Type J stabilizer

6 6 6

Non-proprietary Version

Document No.L5-04GA567(6)

(83/149)

MITSUBISHI HEAVY INDUSTRIES, LTD.

Table 8.2.3-4 In-plane FEI Analysis Results for 2A SG when the thermal power is 80% and 10 consecutive support points are inactive

Tube		Mode	Tube natural frequency	Damping Ratio h(%)				Critical coefficient					Average fluid density	Average void fraction	Maximum void fraction	Critical flow velocity	Effective flow velocity	Stability ratio
Row	Col		f(Hz)	Structural damping	Two phase damping	Squeeze film damping	Total	K1	K_0	K_i	K_θ	K	ρ_0(lb/ft^3)	[-]	[-]	Uc(ft/sec)	Ue(ft/sec)	
80	70																	
80	80																	
100	70																	
100(*)	80(*)																	
120	70																	
120	80																	
95(*)	85(*)																	
125	85																	
138	84																	

Note(*): Plugged tube with Type J stabilizer

6 6 6

Non-proprietary Version

Document No.L5-04GA567(6)

(84/149)

MITSUBISHI HEAVY INDUSTRIES, LTD.

Table 8.2.3-5 In-plane FEI Analysis Results for 2A SG when the thermal power is 90% and 10 consecutive support points are inactive

Tube		Mode	Tube natural frequency	Damping Ratio h(%)				Critical coefficient					Average fluid density	Average void fraction	Maximum void fraction	Critical flow velocity	Effective flow velocity	Stability ratio
Row	Col		f(Hz)	Structural damping	Two phase damping	Squeeze film damping	Total	K1	K_0	K_i	K_θ	K	ρ_0(lb/ft^3)	[-]	[-]	Uc(ft/sec)	Ue(ft/sec)	
80	70																	
80	80																	
100	70																	
100(*)	80(*)																	
120	70																	
120	80																	
95(*)	85(*)																	
125	85																	
138	84																	

Note(*): Plugged tube with Type J stabilizer

6 6 6

Non-proprietary Version

Document No.L5-04GA567(6)

(85/149)

MITSUBISHI HEAVY INDUSTRIES, LTD.

Table 8.2.3-6 In-plane FEI Analysis Results for 2A SG when the thermal power is 100% and 10 consecutive support points are inactive

Tube		Mode	Tube natural frequency	Damping Ratio h(%)				Critical coefficient					Average fluid density	Average void fraction	Maximum void fraction	Critical flow velocity	Effective flow velocity	Stability ratio
Row	Col		f(Hz)	Structural damping	Two phase damping	Squeeze film damping	Total	K1	K_0	K_i	K_θ	K	ρ_0(lb/ft^3)	[-]	[-]	Uc(ft/sec)	Ue(ft/sec)	
80	70																	
80	80																	
100	70																	
100(*)	80(*)																	
120	70																	
120	80																	
95(*)	85(*)																	
125	85																	
138	84																	

Note(*): Plugged tube with Type J stabilizer

6

6

6

Non-proprietary Version

Document No.L5-04GA567(6)

(86/149)

MITSUBISHI HEAVY INDUSTRIES, LTD.

Table 8.2.3-7 In-plane FEI Analysis Results for no plugging model when the thermal power is 100% and 10 consecutive support points are inactive

Tube		Mode	Tube natural frequency	Damping Ratio h(%)				Critical coefficient					Average fluid density	Average void fraction	Maximum void fraction	Critical flow velocity	Effective flow velocity	Stability ratio
Row	Col		f(Hz)	Structural damping	Two phase damping	Squeeze film damping	Total	K1	K_0	K_i	K_θ	K	ρ_0(lb/ft^3)	[-]	[-]	Uc(ft/sec)	Ue(ft/sec)	
80	70																	
80	80																	
100	70																	
100	80																	
120	70																	
120	80																	
95	85																	
125	85																	
138	84																	

Table 8.2.4-1 In-plane FEI Analysis Results for 2A SG when the thermal power is 50% and all consecutive support points are inactive

Tube		Mode	Tube *natural* frequency	Damping Ratio h(%)				Critical coefficient					Average *fluid* density	Average *void* fraction	Maximum *void* fraction	Critical *flow* velocity	Effective *flow* velocity	Stability ratio
Row	Col		f(Hz)	Structural damping	Two phase damping	Squeeze film damping	Total	K1	K_0	K_i	K_θ	K	ρ_0(lb/ft^3)	[-]	[-]	Uc(ft/sec)	Ue(ft/sec)	
80	70																	
80	80																	
100	70																	
100(*)	80(*)																	
120	70																	
120	80																	
95(*)	85(*)																	
125	85																	
138	84																	

Note(*): Plugged tube with Type J stabilizer

6 6 6

Non-proprietary Version

Document No.L5-04GA567(6)

(88/149)

MITSUBISHI HEAVY INDUSTRIES, LTD.

Table 8.2.4-2 In-plane FEI Analysis Results for 2A SG when the thermal power is 60% and all consecutive support points are inactive

Tube		Mode	Tube natural frequency	Damping Ratio h(%)				Critical coefficient					Average fluid density	Average void fraction	Maximum void fraction	Critical flow velocity	Effective flow velocity	Stability ratio
Row	Col		f(Hz)	Structural damping	Two phase damping	Squeeze film damping	Total	K1	K_0	K_i	K_θ	K	ρ_0(lb/ft^3)	[-]	[-]	Uc(ft/sec)	Ue(ft/sec)	
80	70																	
80	80																	
100	70																	
100(*)	80(*)																	
120	70																	
120	80																	
95(*)	85(*)																	
125	85																	
138	84																	

Note(*): Plugged tube with Type J stabilizer

6 6 6

Non-proprietary Version

Document No.L5-04GA567(6)

(89/149)

MITSUBISHI HEAVY INDUSTRIES, LTD.

Table 8.2.4-3 In-plane FEI Analysis Results for 2A SG when the thermal power is 70% and all consecutive support points are inactive

Tube		Mode	Tube natural frequency	Damping Ratio h(%)				Critical coefficient					Average fluid density	Average void fraction	Maximum void fraction	Critical flow velocity	Effective flow velocity	Stability ratio
Row	Col		f(Hz)	Structural damping	Two phase damping	Squeeze film damping	Total	K1	K_0	K_i	K_θ	K	ρ_0(lb/ft^3)	[-]	[-]	Uc(ft/sec)	Ue(ft/sec)	
80	70																	
80	80																	
100	70																	
100(*)	80(*)																	
120	70																	
120	80																	
95(*)	85(*)																	
125	85																	
138	84																	

Note(*): Plugged tube with Type J stabilizer

6 6 6

Non-proprietary Version

Document No.L5-04GA567(6)

(90/149)

MITSUBISHI HEAVY INDUSTRIES, LTD.

Table 8.2.4-4 In-plane FEI Analysis Results for 2A SG when the thermal power is 80% and all consecutive support points are inactive

Tube		Mode	Tube natural frequency	Damping Ratio h(%)				Critical coefficient					Average fluid density	Average void fraction	Maximum void fraction	Critical flow velocity	Effective flow velocity	Stability ratio
Row	Col		f(Hz)	Structural damping	Two phase damping	Squeeze film damping	Total	K1	K_0	K_i	K_θ	K	ρ_0(lb/ft^3)	[-]	[-]	Uc(ft/sec)	Ue(ft/sec)	
80	70																	
80	80																	
100	70																	
100(*)	80(*)																	
120	70																	
120	80																	
95(*)	85(*)																	
125	85																	
138	84																	

Note(*): Plugged tube with Type J stabilizer

6 6 6

Non-proprietary Version

Document No.L5-04GA567(6) (91/149)

MITSUBISHI HEAVY INDUSTRIES, LTD.

Table 8.2.4-5 In-plane FEI Analysis Results for 2A SG when the thermal power is 90% and all consecutive support points are inactive

Tube		Mode	Tube natural frequency	Damping Ratio h(%)				Critical coefficient					Average fluid density	Average void fraction	Maximum void fraction	Critical flow velocity	Effective flow velocity	Stability ratio
Row	Col		f(Hz)	Structural damping	Two phase damping	Squeeze film damping	Total	K1	K_0	K_i	K_θ	K	ρ_0(lb/ft^3)	[-]	[-]	Uc(ft/sec)	Ue(ft/sec)	
80	70																	
80	80																	
100	70																	
100(*)	80(*)																	
120	70																	
120	80																	
95(*)	85(*)																	
125	85																	
138	84																	

Note(*): Plugged tube with Type J stabilizer

6 6 6

Non-proprietary Version

Document No.L5-04GA567(6)

Table 8.2.4-6 In-plane FEI Analysis Results for 2A SG when the thermal power is 100% and all consecutive support points are inactive

Tube		Mode	Tube natural frequency	Damping Ratio h(%)				Critical coefficient					Average fluid density	Average void fraction	Maximum void fraction	Critical flow velocity	Effective flow velocity	Stability ratio
Row	Col		f(Hz)	Structural damping	Two phase damping	Squeeze film damping	Total	K1	K_o	K_i	K_θ	K	ρ_0(lb/ft^3)	[-]	[-]	Uc(ft/sec)	Ue(ft/sec)	
80	70																	
80	80																	
100	70																	
100(*)	80(*)																	
120	70																	
120	80																	
95(*)	85(*)																	
125	85																	
138	84																	

Note(*): Plugged tube with Type J stabilizer

6 6 6

Non-proprietary Version

Document No.L5-04GA567(6) (93/149)

MITSUBISHI HEAVY INDUSTRIES, LTD.

Table 8.2.4 -7 In-plane FEI Analysis Results for no plugging model when the thermal power is 100% and all consecutive support points are inactive

Tube		Mode	Tube natural frequency	Damping Ratio h(%)				Critical coefficient					Average fluid density	Average void fraction	Maximum void fraction	Critical flow velocity	Effective flow velocity	Stability ratio
Row	Col		f(Hz)	Structural damping	Two phase damping	Squeeze film damping	Total	K1	K_0	K_i	K_θ	K	ρ_0(lb/ft^3)	[-]	[-]	Uc(ft/sec)	Ue(ft/sec)	
80	70																	
80	80																	
100	70																	
100	80																	
120	70																	
120	80																	
95	85																	
125	85																	
138	84																	

9. Reference

1) ASME Boiler and Pressure Vessel Code, Sec II, Materials, 1998 Edition through 2000 addenda.
2) ASME Boiler and Pressure Vessel Code, Sec III Appendix N-1330, 1998 Edition through 2000 addenda.
3) L5-04FU001 the latest revision, Component and Outline Drawing 1/3
4) L5-04FU002 the latest revision, Component and Outline Drawing 2/3
5) L5-04FU003 the latest revision, Component and Outline Drawing 3/3
6) L5-04FU021 the latest revision, Tube Sheet and Extension Ring 1/3
7) L5-04FU022 the latest revision, Tube Sheet and Extension Ring 2/3
8) L5-04FU023 the latest revision, Tube Sheet and Extension Ring 3/3
9) L5-04FU051 the latest revision, Tube Bundle 1/3
10) L5-04FU052 the latest revision, Tube Bundle 2/3
11) L5-04FU053 the latest revision, Tube Bundle 3/3
12) L5-04FU111 the latest revision, AVB assembly 1/9
13) L5-04FU112 the latest revision, AVB assembly 2/9
14) L5-04FU113 the latest revision, AVB assembly 3/9
15) L5-04FU114 the latest revision, AVB assembly 4/9
16) L5-04FU115 the latest revision, AVB assembly 5/9
17) L5-04FU116 the latest revision, AVB assembly 6/9
18) L5-04FU117 the latest revision, AVB assembly 7/9
19) L5-04FU118 the latest revision, AVB assembly 8/9
20) L5-04FU119 the latest revision, AVB assembly 9/9
21) Analysis of Thermal Hydraulics of Steam Generators/Steam Generator Analysis Package, Ver.3.1, 1016564, EPRI.
22) L5-04GA566 the latest revision, Case study of the input parameters and tube plugging impact on internal SG thermal hydraulics parameters
23) Connors, H.J., Fluid Elastic Vibration of Tube Arrays Excited by Cross Flow, ASME Annual Meeting, 1970.
24) Blevins, R. D., "Flow-induced Vibration", Krieger Publishing Company.
25) M.J. Pettigrew.,et.al.,2011,Damping of Heat Exchanger Tubes in Liquids: Review and Design Guidelines,Journal of Pressure Vessel Technology Vol.133
26) M.J. Pettigrew.,et.al.,2003,"Vibration analysis of shell-and-tube heat exchangers" Journal of Fluids and Structures 18 (2003) 469-483
27) S. M. Fluit and M. J. Pettigrew, "Simplified method for predicting vibration and fretting-wear in nuclear steam generator U-bend tube bundle", ASME PVP 2001 Vol.420-1
28) WJS16263, MHI Test Report of Fluid Elastic Vibration
29) M.J. Pettigrew.,et.al.,2000, "The effects of tube bundle geometry on vibration in two-phase cross-flow",Flow Induced Vbration, Ziada&Staubi(eds) 2000 Balkema, Rotterdam ISBN9058091295
30) Flow-Induced Vibration,Meskell & Bennett (eds) ISBN 978-0-9548583-4-6, "Study on In-flow Fluid-elastic Instability of Circular Cylinder Arrays"], T.Nakamura, Y.Fujita, T.Oyakawa, Y.NI. July 2012
31) H.C.Yeung, 1983, "The effect of Approach Flow Direction on the Flow-Induced Vibrations of a Triangular Tube Array", Transaction of ASME Vol.105
32) L5-04GA587 the latest revision, Test result for damping ratio added by the stabilizer inserted for short length (Row No. 106)

△6

Attachment-1

Computer Input and Output File List

Table I-1 Input and Output file name of out of plane FEI evaluation for 2A SG when all support points are active 6

Thermal Power(%)	Row	Column	Input [1)]	Output [1)]
70	80	70	[	]
	80	80		
	100	70		
	100	80		
	120	70		
	120	80		
	95	85		
	125	85		
	138	84		
100 (No Plug)	80	70		
	80	80		
	100	70		
	100	80		
	120	70		
	120	80		
	95	85		
	125	85		
	138	84		

Table I-2 Input and Output file name of out of plane FEI evaluation for 2A SG when 1 support points are inactive 6

Thermal Power(%)	Row	Column	Input [1)]	Output [1)]
70	80	70	[	]
	80	80		
	100	70		
	100	80		
	120	70		
	120	80		
	95	85		
	125	85		
	138	84		
100 (No Plug)	80	70		
	80	80		
	100	70		
	100	80		
	120	70		
	120	80		
	95	85		
	125	85		
	138	84		

Notes:

1) All files are saved in the directory as below:

[ ] 6

Table I-3 Input and Output file name of in-plane FEI evaluation for 2A SG when 6 consecutive support points are inactive (1/2) 6

Thermal Power(%)	Row	Column	Input [1)]	Output [1)]
50	80	70		
	80	80		
	100	70		
	100	80		
	120	70		
	120	80		
	95	85		
	125	85		
	138	84		
60	80	70		
	80	80		
	100	70		
	100	80		
	120	70		
	120	80		
	95	85		
	125	85		
	138	84		
70	80	70		
	80	80		
	100	70		
	100	80		
	120	70		
	120	80		
	95	85		
	125	85		
	138	84		
80	80	70		
	80	80		
	100	70		
	100	80		
	120	70		
	120	80		
	95	85		
	125	85		
	138	84		
90	80	70		
	80	80		
	100	70		
	100	80		
	120	70		
	120	80		
	95	85		
	125	85		
	138	84		
100	80	70		
	80	80		
	100	70		
	100	80		
	120	70		
	120	80		
	95	85		
	125	85		
	138	84		

Notes: 1) All files are saved in the directory as below: 6

Table I-3 Input and Output file name of in-plane FEI evaluation for 2A SG when 6 consecutive support points are inactive (2/2) 6

Thermal Power(%)	Row	Column	Input [1)]	Output [1)]
100 (No Plug)	80	70	[	]
	80	80		
	100	70		
	100	80		
	120	70		
	120	80		
	95	85		
	125	85		
	138	84	[	]

Notes: 1) All files are saved in the directory as below:

Table I-4 Input and Output file name of in-plane FEI evaluation for 2A SG when 8 consecutive support points are inactive (1/2) 6

Thermal Power(%)	Row	Column	Input [1)]	Output [1)]
50	80	70		
	80	80		
	100	70		
	100	80		
	120	70		
	120	80		
	95	85		
	125	85		
	138	84		
60	80	70		
	80	80		
	100	70		
	100	80		
	120	70		
	120	80		
	95	85		
	125	85		
	138	84		
70	80	70		
	80	80		
	100	70		
	100	80		
	120	70		
	120	80		
	95	85		
	125	85		
	138	84		
80	80	70		
	80	80		
	100	70		
	100	80		
	120	70		
	120	80		
	95	85		
	125	85		
	138	84		
90	80	70		
	80	80		
	100	70		
	100	80		
	120	70		
	120	80		
	95	85		
	125	85		
	138	84		
100	80	70		
	80	80		
	100	70		
	100	80		
	120	70		
	120	80		
	95	85		
	125	85		
	138	84		

Notes: 1) All files are saved in the directory as below:

Table I-4 Input and Output file name of in-plane FEI evaluation for 2A SG when 8 consecutive support points are inactive (2/2) 6

Thermal Power(%)	Row	Column	Input [1)]	Output [1)]
100 (No Plug)	80	70	[	]
	80	80		
	100	70		
	100	80		
	120	70		
	120	80		
	95	85		
	125	85		
	138	84		

Notes: 1) All files are saved in the directory as below: 6

Table I-5 Input and Output file name of in-plane FEI evaluation for 2A SG when 10 consecutive support points are inactive (1/2) 6

Thermal Power(%)	Row	Column	Input [1)]	Output [1)]
50	80	70		
	80	80		
	100	70		
	100	80		
	120	70		
	120	80		
	95	85		
	125	85		
	138	84		
60	80	70		
	80	80		
	100	70		
	100	80		
	120	70		
	120	80		
	95	85		
	125	85		
	138	84		
70	80	70		
	80	80		
	100	70		
	100	80		
	120	70		
	120	80		
	95	85		
	125	85		
	138	84		
80	80	70		
	80	80		
	100	70		
	100	80		
	120	70		
	120	80		
	95	85		
	125	85		
	138	84		
90	80	70		
	80	80		
	100	70		
	100	80		
	120	70		
	120	80		
	95	85		
	125	85		
	138	84		
100	80	70		
	80	80		
	100	70		
	100	80		
	120	70		
	120	80		
	95	85		
	125	85		
	138	84		

Notes: 1) All files are saved in the directory as below:

6

Table I-5 Input and Output file name of in-plane FEI evaluation for 2A SG when 10 consecutive support points are inactive (2/2) 6

Thermal Power(%)	Row	Column	Input [1)]	Output [1)]
100 (No Plug)	80	70	[	]
	80	80		
	100	70		
	100	80		
	120	70		
	120	80		
	95	85		
	125	85		
	138	84	[	]

Notes: 1) All files are saved in the directory as below:

Table I-6 Input and Output file name of in-plane FEI evaluation for 2A SG when 12 consecutive support points are inactive (1/2) 6

Thermal Power(%)	Row	Column	Input [1)]	Output [1)]
50	80	70		
	80	80		
	100	70		
	100	80		
	120	70		
	120	80		
	95	85		
	125	85		
	138	84		
60	80	70		
	80	80		
	100	70		
	100	80		
	120	70		
	120	80		
	95	85		
	125	85		
	138	84		
70	80	70		
	80	80		
	100	70		
	100	80		
	120	70		
	120	80		
	95	85		
	125	85		
	138	84		
80	80	70		
	80	80		
	100	70		
	100	80		
	120	70		
	120	80		
	95	85		
	125	85		
	138	84		
90	80	70		
	80	80		
	100	70		
	100	80		
	120	70		
	120	80		
	95	85		
	125	85		
	138	84		
100	80	70		
	80	80		
	100	70		
	100	80		
	120	70		
	120	80		
	95	85		
	125	85		
	138	84		

Notes: 1) All files are saved in the directory as below:

Table I -6 Input and Output file name of in-plane FEI evaluation for 2A SG when 12 consecutive support points are inactive (2/2) 6

Thermal Power(%)	Row	Column	Input [1)]	Output [1)]
100 (No Plug)	80	70	[	]
	80	80		
	100	70		
	100	80		
	120	70		
	120	80		
	95	85		
	125	85		
	138	84		

Notes: 1) All files are saved in the directory as below: 6

Attachment-2 Evaluation of Liquid Film Thickness of Tube at AVB Support Point

1. Summary

In order to estimate the effect of void fraction on the squeeze film damping, the relation between the liquid film thickness of tube at each AVB support point and void fraction is evaluated as shown in Table-1.

Table-1 Relation between liquid film thickness of tube and void fraction

Void fraction	Liquid Film	Condition	Figure
[	No	Dry out	Fig.1-1
	Discontinuous	Dry & Wet	Fig.1-2
]	Continuous	Wet	Fig.1-3

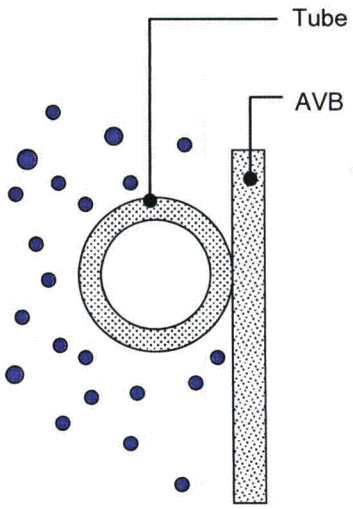

Fig.1-1 No film (Dry out)

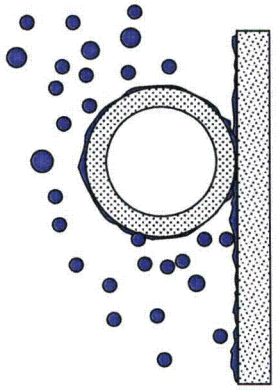

Fig.1-2 Discontinuous (Dry & Wet)

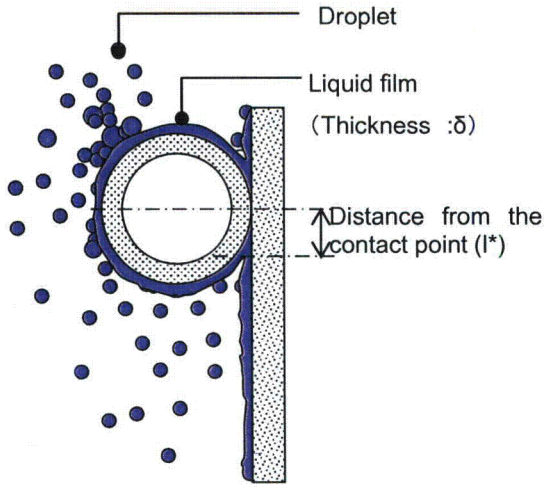

Fig.1-3 Continuous (Wet)

The boundary of void fraction is determined as follows and the flow regime is confirmed to be consistent with the figures above as described in Attachment-4.

2. Assumption of Liquid Film Thickness

Fig.2 shows the relation between distance from the contact point (l*) and liquid film thickness (δ), which is obtained by the following geometrical equation, where θ and d are defined in Fig.3.

$$\frac{d}{2}(1-\cos\theta) \cong 2\delta \qquad (1)$$

$$l^* = \frac{d}{2}\sin\theta \qquad (2)$$

- The thickness of the continuous liquid film is [ ] which is obtained in Fig.2 by assuming the effective distance from the contact point for squeeze film damping is [ ] [ ] The basis of [ ] of the effective distance is described in Attachment-3.
- The minimum thickness of discontinuous liquid film is assumed to be [ ] which is comparable to the degree of surface roughness of tube.

[ ]

Fig.2 Relation between distance from the contact point and liquid film thickness

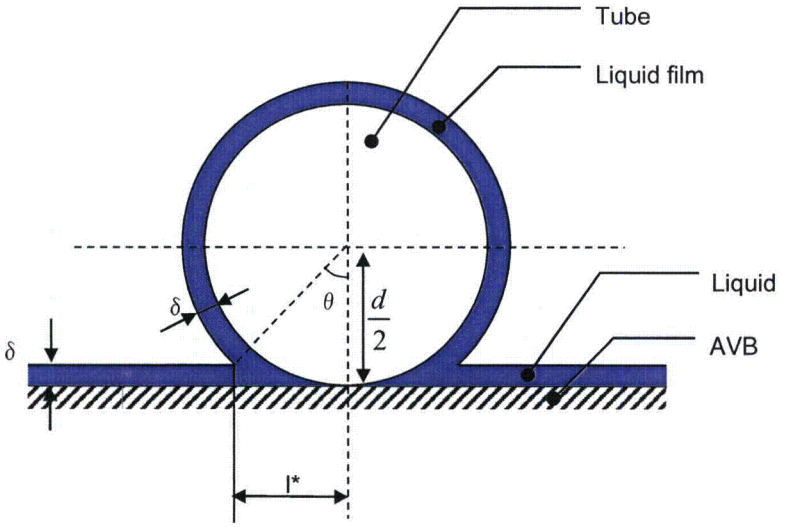

Fig.3 Distance from the contact point and liquid film thickness

3. Estimation of Void fraction

Fig.4 shows the relation between void fraction and liquid film thickness, which is obtained from the following equations.

$$\alpha = \frac{A_{sub} - (A_f + A_d)}{A_{sub}} \quad (3)$$

$$A_f = \frac{\pi}{4} \cdot \left[(d + 2\delta)^2 - d^2 \right] \quad (4)$$

$$A_d = \frac{1}{2} A_f \quad (5)$$

$$A_{sub} = \frac{\sqrt{3}}{2} Pt^2 - \frac{\pi}{4} d^2 \quad (6)$$

Where,

α : Void fraction

Pt : Tube pitch

d : Tube diameter

A_{sub} : Flow area of sub channel (See Fig.5)

A_d : Sectional area of droplet (See Fig.5)

A_f : Sectional area of liquid film, which is assumed to be a twice of the area of droplet (See Fig.5) and the basis of this assumption is described as follows.

The ratio between the flow rate of liquid film G_f and the flow rate of droplet G_E can be assumed to be 0.2 in accordance with the test results shown in Fig.6 (Ref.1).

Fig.6 is the results of heating cylinder which indicates that the flow rate of liquid film, G_f, is approximately 20% of the flow rate of droplet, G_E, when the quality is 50%.(50% quality at SONGS RSG condition (steam pressure is 838 psia) corresponds to 91% of void fraction)..

$$\frac{G_f}{G_E} = \sim \frac{1}{5} \quad (7)$$

On the other hand, the ratio between the flow velocity of droplet, U_e, and the flow velocity of liquid film, U_f, is approximately 10, which is obtained from Fig.7.

Fig.7 is the air-water flow test results of cylinder at atmospheric condition where the flow velocity of liquid film and the apparent gas velocity are measured in various conditions of the apparent liquid velocity, j_l, and the hydraulic equivalent diameter (Ref.2). Since ratio between the flow velocity of liquid film and droplet does not depend on the pressure (Ref.3), these data are applicable to SONGS RSG

evaluation.

Assuming the velocity of the droplet, U_e, is identical to the apparent gas velocity, j_g, the flow velocity of droplet, U_e, is approximately ten times the flow velocity of liquid film, U_f, at all conditions. The flow velocity of the liquid film does not depend on the condition of the apparent liquid velocity or the hydraulic equivalent diameter.

$$\frac{u_e}{u_f} \cong \frac{j_g}{u_f} \cong 10 \qquad (8)$$

From the equation of continuity (9), the ratio of sectional area between liquid film and droplet can be derived as follows. (Equation (10) is identical to Equation (5))

$$\frac{G_f}{G_E} = \frac{\rho_f Q_f}{\rho_f Q_E} = \frac{Q_f}{Q_E} = \frac{A_f \cdot u_f}{A_d \cdot u_E} \qquad (9)$$

$$\frac{A_f}{A_d} = \frac{Q_f}{Q_E} \cdot \frac{u_E}{u_f} \cong 2 \qquad (10)$$

Fig.4 indicates;

- When void fraction is lower than 95%, there is a continuous liquid film on the tube since the thickness of liquid film is larger than[ ]
- When void fraction is higher than 98%, there is no liquid film on the tube since the thickness of liquid film is smaller than[ ]which is the assumed minimum thickness of the discontinuous liquid film on the tube.

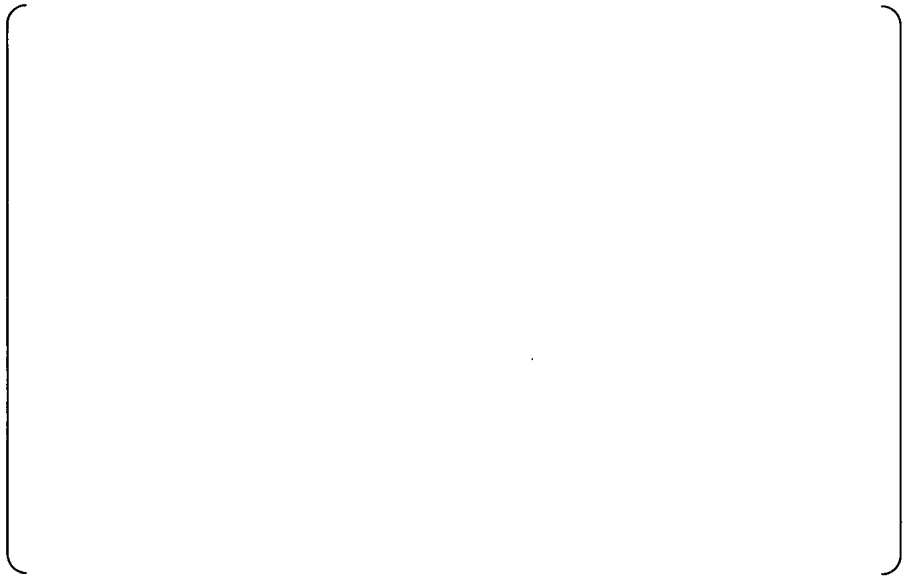

Fig.4 Relation between void fraction and liquid film thickness

4. References

1) Akagawa,"Gas and liquid Two-phase Flow" p.150

2) "Fluid characteristics of annular mist flow of gas and liquid" p.395-495, 49-438

3) Nakazatomi, et.al, Experimental study of vertical upward gas-liquid two-phase annular flow (2nd report, effects of system pressure on characteristics of waves)

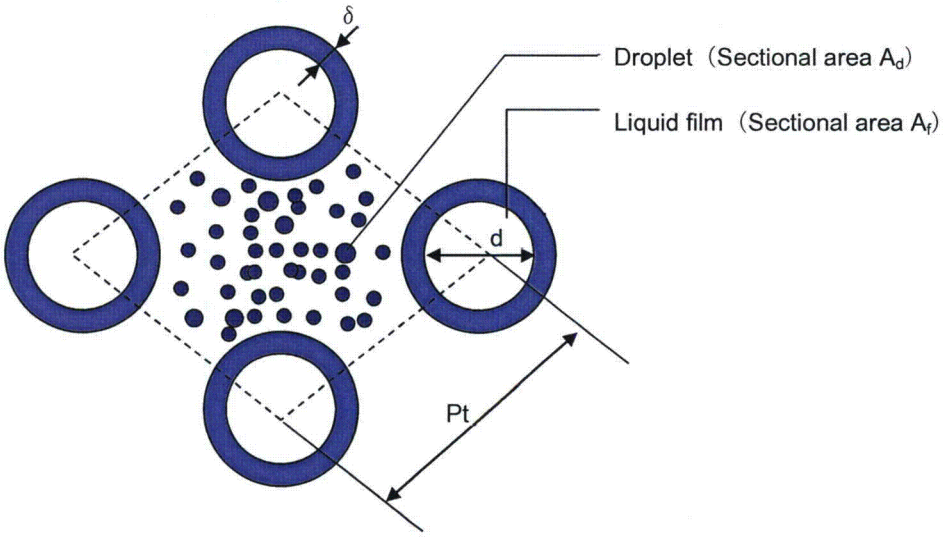

Fig. 5 Sectional area of droplet and liquid film

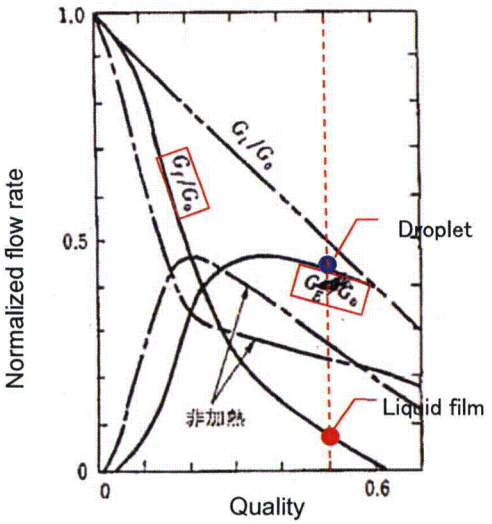

G_f is approximately 20 % of G_E when the quality is 0.5

Test condition

- Two-phase flow (steam/water) in heating cylinder (heat flix is 8.6 $\times 10^4$ W/ft^2)
- At high pressure (427psia)

Fig.6 Flow rate of liquid film and droplet (Ref.1)

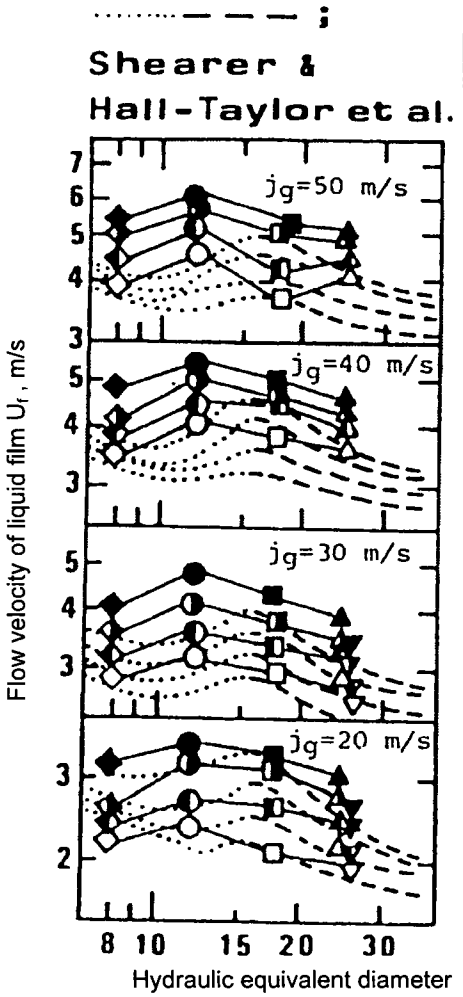

U_f is approximately 10 % of J_g in all cases, which does not depend on J_l and the hydraulic equivalent diameter

Test condition

- Water/air flow in a cylinder
- At atmospheric pressure and room temperature

Definition of symbols

J_l m/s \ D mm	8	12	18	25	26
0.04	◇	○	□	△	▽
0.06	◆	◐	◧	▲	▼
0.1	◆	◑	◨	▲	▼
0.14	◆	●	■	▲	▼

Fig.7 Flow rate of liquid film and droplet (Ref.2)

Attachment-3 Evaluation of the Effective Distance of Liquid Film of Tube from the Contact Point for Squeeze Film Damping

The effective distance of liquid film of tube from the contact point for squeeze film damping is evaluated to be [ ] as calculated below.

The calculation model of tube and AVB is shown in Fig.1. When the amplitude of gap velocity vibration in normal direction of AVB is v_0, the velocity at x in horizontal direction is defined as equation (1) since the liquid volume pushed out by the tube is the same as the liquid volume which flows in the horizontal direction.

$$v(x) = \frac{v_0}{\delta(x)} \tag{1}$$

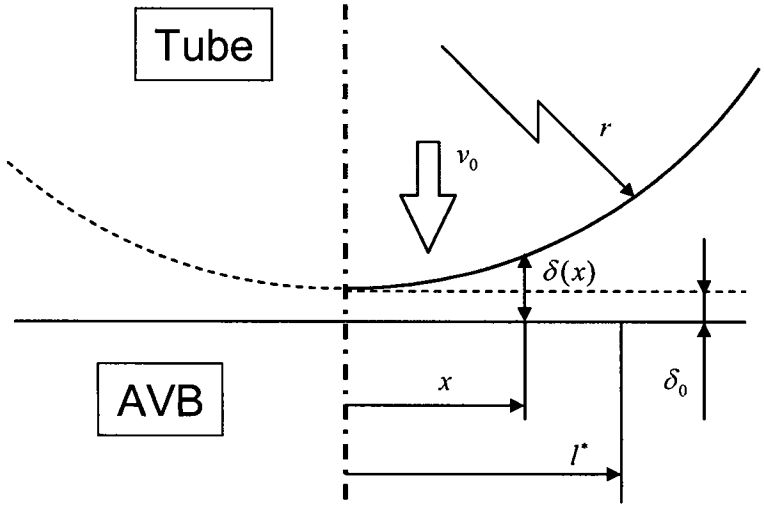

Fig.1 Calculation model

On the other hand, the force balance of the small volume in the gap flow area is presented as equation (2).

$$\frac{v^2}{2}+\frac{p}{\rho}=\frac{v(x+dx)^2}{2}+\frac{p(x+dx)}{\rho}+\frac{v^2 dx}{2\delta}\lambda \quad (2)$$

Where,

p :Pressure

ρ :Liquid density

λ :Tube friction factor defined by equation (3).

$$\lambda=\begin{cases}48/\mathrm{Re} & if \quad \mathrm{Re}<1300\\ 0.26\,\mathrm{Re}^{-0.24} & if \quad \mathrm{Re}>1300\end{cases} \quad (3)$$

The equation (4) represents the pressure gradient, which is derived by differentiating the equation (3).

$$\frac{dp}{dx}=-\frac{\rho}{2}\frac{dv^2}{dx}-\frac{\rho v(x)^2}{2}\frac{\lambda(\mathrm{Re})}{2\delta(x)} \quad (4)$$

The pressure at x is shown as equation (5), which is obtained by integrating equation (4).

$$p(x)=\frac{\rho v(x)^2}{2}-\int_0^x\left(\frac{\rho v(x)^2}{2}+\frac{\lambda(\mathrm{Re})}{\delta(x)}\right)dx+p_0 \quad (5)$$

Since the shape of the gap flow area is divergent and the flow velocity at the exit of the gap flow area is negligibly small, P_0 can be determined by assuming that the hydraulic pressure is zero.

The damping force Fd is presented in equation (6), which is derived by integrating pressure.

$$F=2H\int_0^{l^*}p(x)dx \quad (6)$$

Where,

H : AVB width

l^* : Effective distance of liquid film of tube from the contact point

Therefore, the damping coefficient C_d is,

$$C_d=F/v_0 \quad (7)$$

Fig.2 shows the calculation results of the normalized damping coefficient which is a fraction to the maximum value obtained by using the equations above and the conditions listed in Table1.

Fig.2 indicates a trend that when the distance from the contact point is greater than [ ] the damping coefficient will be saturated.

Table 1 Conditions

Initial gap	
Tube diameter	
AVB width	
Amplitude of displacement	
Frequency of vibration	
Liquid density	
Kinetic viscosity	

Note *: Values at BOL design condition (Th=598 deg.F)

Distance from the contact point (mm)

Fig.2 The damping coefficient and the distance from the contact point

Attachment-4 Confirmation of Flow Regime

1. Flow regime

MHI has calculated the Grant flow regime map as shown in Figure1 by using ATHOS computer code outputs of BOL design condition[ ] in accordance with Reference 1. 12 tubes shown in Figure 1 are selected as representatives and each tube has 19 evaluation points in U-bend (10 degrees pitch data such as 0, 10, 20, ..., 180 degrees).

The points at hot side (0, 10, 20, ...,90* degrees) are shown as filled markers and the points at cold side (100, 110, 120,...,180 degrees) are shown as non-filled markers in Figure 1. Most plots on the hot side are in the spray flow regime, which is consistent with the methodology of the squeeze film evaluation.

2. Reference

[1] M. Pettigrew and C. Taylor, "Vibration Analysis of shell-and-tube heat exchangers: an overview–Part I: Flow, Damping, Fluidelastic Instability," Journal of Fluids and Structures 18 (2003) 469-483

[ ]

Note *: The points at 90 degrees are included in the hot side.

Figure 1 Flow Regime of Representative Tubes at BOL Design Condition

Attachment-5 Case Study for Applying Split Stabilizers for TTW tube of Unit-2 at 70% Thermal Power

1. Purpose

The purpose of this attachment is to confirm the effectiveness of applying the split stabilizers for TTW (tube-to-tube wear) tubes. In order to confirm the effectiveness of the split stabilizers, some cases shown in Table 2-1 are studied. △6

2. Conclusion

The results of case study for applying type J stabilizer are shown in Table 2-1 and Figure 2-1. Type J stabilizers are split stabilizers that extend approximately 60° into the U-bend, inserted on the hot and cold side of the tube. It has been confirmed that stability ratio of TTW tubes with type J stabilizer is less than 1.0. △6

Table 2-1 Natural Frequency and Stability Ratio

Tube	Without Stabilizer		With split Stabilizers (To 60 degrees in U-bend at both of hot and cold side)							
			Small amplitude Additional damping ratio		Medium amplitude Additional damping ratio		Large amplitude Additional damping ratio		Very large amplitude Additional damping ratio	
	Natural Frequency (Hz)	Stability Ratio	Natural Frequency (Hz)	Stability Ratio	Natural Frequency (Hz)	Stability Ratio	Natural Frequency (Hz)	Stability Ratio	Natural Frequency (Hz)	Stability Ratio
R111C81										
R113C81										

(a) Relationship between stability ratio and additional damping (b) Relationship between stability ratio and tube amplitude (R113C81)

Fig. 2-1 Effect of additional damping on the stability ratio

3. Assumption

(1) Representative tube

Representative tubes (Row113 Col.81 and Row111 Col.81) are TTW tubes of Unit-2 (2 tubes).

(2) AVB support points

In this evaluation, all AVB support points are assumed to be inactive for conservatism because the stability ratios of the tubes obtained from the evaluation will be the maximum possible values.

(3)Plugging and Stabilizer

The representative tubes are assumed to be plugged with or without split stabilizers.

In the cases with split stabilizers, the stabilizers are assumed to be installed to 60 degrees in the U-bend region at the both of hot and cold side to maximize the structural damping. As shown in Table 3-1, the additional damping ratio by the split stabilizers (Type J) is assumed to be the difference between the damping ratio of tube with and without split stabilizers based on the report of the damping test (Ref.32). Table 3-1 was derived for Row 106 but can be applied to all rows. △6

Table 3-1 Additional damping due to split stabilizers △6

Amplitude	Damping ratio (%)		
	Without stabilizer	With split stabilizers	Additional damping ratio
Small			
Medium			
Large			
Very large			

(4) Effect of primary water entering into the TTW tubes

The effect of primary water entering into the TTW tubes is not taken into account by assuming there in no leakage through the plugging.

4. Acceptance criteria

There are no criteria because of parametric case study.

5. Design inputs

5.1 Geometry

The tube bundle consists of| |diameter, thermally treated Alloy 690 U-tubes that are arranged in a | |equilateral triangular pitch and are supported by the tubesheet, seven tube support plates, and six sets of anti-vibration bars (AVBs). Tube support plates (TSPs) have broached trifoil tube holes. All the contacting support structures above the tubesheet are made of 405 stainless steel. The nominal dimension of tube, TSPs and AVBs are listed in Table 5-1.

5.2 Thermal and Hydraulic flow of steam generator secondary side

The ATHOS thermal hydraulic analysis program was used to determine the distributions of fluid gap velocity in the normal direction to tube in-plane and fluid density. Table 5-2 and Fig 5-1, 5-2 show the flow characteristic that are applied to the tubes for the evaluation at 70% thermal power of Unit-2 with plugging.

6. Methodology

The analysis is performed in accordance with the same procedures provided in main report to evaluate the best estimated stability ratio for in-plane FEI. 6

7 Results

The analysis results are shown in Table 7-1 and 7-2.

Table 5-1 Nominal dimensions of tubes, TSPs, and AVBs

Part	Item	Value
Tubes	Material	Thermally treated SB-163 UNS N06690
	Outside diameter	0.75 in
	Thickness	0.043 in
	Number of tubes	9727
	Tube pitch	1.0 in
	Tube arrangement	Triangular
TSPs	Material	SA-240 Type 405
	Thickness	
	Number of TSPs	
	Tube support span (between TSP centers)	
	Tube support span (from tubesheet to TSP-1)	
AVBs	Material	SA-479 Type 405
	Type	
	Thickness	
	Width	
Stabilizer	Unit weight	

6

Table 5-2 Basic parameters for calculation for 2A SG evaluation after plugging

Plugging	305
Thermal power (MWt)	1213.3 (70%)
RCS flow rate (gpm)	206,695
T_{hot} (Tsg-in) (°F)	
$T_{sg\text{-}out}$ (°F)	
T_{cold} (°F)	
Saturation Steam Pressure (psia)	
Fouling Factor ($ft^2hr°F$ /Btu)	
$T_{feedwater}$ (°F)	
Circulation Ratio	
Steam Mass Flow (lb/hr)	
Feed Water Mass Flow (lb/hr)	
Blowdown flow rate (gpm)	

Fig. 5-1 Flow Characteristics of Row111 Col81

Fig. 5-2 Flow Characteristic of Row 113 Col.81

Table 7-1 Analysis results for case study of split stabilizers (Row 111 Column 81) 6

Tube condition	Additional Structural damping (%)	Mode	Tube natural frequency f(Hz)	Damping Ratio h(%)				Critical coefficient					Average fluid density ρ_0(lb/ft^3)	Average void fraction [-]	Maximum void fraction [-]	Critical flow velocity Uc(ft/sec)	Effective flow velocity Ue(ft/sec)	Stability ratio
				Structural damping	Two phase damping	Squeeze film damping	Total	K1	K_0	K_i	K_θ	K						
Plugged without stabilizer																		
Plugged with split stabilizers when tube amplitude is small																		
Plugged with split stabilizers when tube amplitude is medium																		
Plugged with split stabilizers when tube amplitude is large																		
Plugged with split stabilizers when tube amplitude is very large																		

Table 7-2 Analysis results for case study of stabilizer (Row 113 Column 81) 6

Tube condition	Additional structural damping (%)	Mode	Tube natural frequency f(Hz)	Damping Ratio h(%)				Critical coefficient					Average fluid density ρ_0(lb/ft^3)	Average void fraction [-]	Maximum void fraction [-]	Critical flow velocity Uc(ft/sec)	Effective flow velocity Ue(ft/sec)	Stability ratio
				Structural damping	Two phase damping	Squeeze film damping	Total	K1	K_0	K_i	K_θ	K						
Plugged without stabilizer																		
Plugged with standard stabilizer																		
Plugged with split stabilizers when tube amplitude is small																		
Plugged with split stabilizers when tube amplitude is medium																		
Plugged with split stabilizers when tube amplitude is large																		
Plugged with split stabilizers when tube amplitude is very large																		

Attachment-6 Uncertainty of Calculated Stability Ratio

1. Purpose

The purpose of this attachment is to evaluate the uncertainty of stability ratio evaluation based on MHI methodology.

2. Summary

The uncertainty of the stability ratio (SR) evaluation based on MHI methodology is evaluated by summing the uncertainties of critical parameters. As a result, the uncertainty of SR evaluation is calculated to be in the range between -5 % and – 57%. Therefore, the stability ratios are calculated conservatively based on MHI methodology.

Table 1 Difference between SR based on MHI evaluation method and best estimated

Relative stability ratio based on MHI evaluation, R^*_{MHI}	Best estimated			Uncertainty of MHI's SR evaluation	
	Mean value	Standard deviation,σ	Mean ±2σ	Upper bound $\frac{SR_{max}}{SR_{MHI}}$	Lower bound $\frac{SR_{min}}{SR_{MHI}}$
[ ]					

3. Evaluation method

In this evaluation, the standard deviation of SR evaluation multiplied by 2 is regarded as an uncertainty. Table 2 shows the parameters used in the SR calculation and includes which parameters should be taken into account. The methodology of the uncertainty evaluation is shown as follows. 6

3.1 Uncertainty of Each Parameter

The uncertainty of each parameter is estimated by the following equation. In this equation, it is assumed that the uncertainty of each parameter is equal to two times as large as standard deviation of relative error.

$$\sigma = \sqrt{\frac{1}{N} \cdot \sum_{i=1}^{N} \left(\frac{X_i - X_{ref}}{X_{ref}} \right)^2} \quad \cdots\cdots (1)$$

Where,

X_{ref} : Reference value of each test data

X_i : test data

σ : Standard deviation of relative error of each test data

N : Number of data

According to error propagation law, the effect of the standard deviation of each parameter on that of SR is evaluated with the following equations (See Ref. 3) and $2\sigma_{SR}$ is regarded as an uncertainty of SR evaluation.

$$\sigma_{SR} = \sqrt{\sigma_p^2 + \sigma_{TH}^2} = \sqrt{\sigma_K^2 + \left(\frac{1}{2}\sigma_\zeta\right)^2 + \sigma_{TH}^2} \quad \cdots\cdots (2)$$

$$\sigma_\zeta = \frac{\sigma_{ST}\zeta_{ST} + \sigma_{TP}\zeta_{TP} + \sigma_{SF}\zeta_{SF}}{\zeta_{ST} + \zeta_{TP} + \zeta_{SF}} = \frac{\sigma_{TP}\zeta_{TP} + \sigma_{SF}\zeta_{SF}}{\zeta} \quad \cdots\cdots (3)$$

$$\sigma_K = \sqrt{\sigma_{K1}^2 + \sigma_a^2} \quad \cdots\cdots (4)$$

Where,

σ_{SR} : Standard deviation of SR uncertainty

σ_{TH} : Standard deviation of SR due to thermal hydraulic parameters evaluation

σ_p : Standard deviation of parameters used for SR evaluation

ζ : Total damping ratio

ζ_{ST} : Structural damping

ζ_{TP} : Two phase damping

ζ_{SF} : Squeeze film damping

σ_ζ : Standard deviation of ζ

σ_{ST} : Standard deviation of ζ_{ST}

σ_{TP} : Standard deviation of ζ_{TP}

σ_{SF} : Standard deviation of ζ_{SF}

σ_K : Standard deviation of K

σ_{K1} : Standard deviation of $K1$

σ_a : Standard deviation of $a(\theta)$

※ Standard deviation noted above (used for SR evaluationeviation of relative error of each parameter (dimensionless)

△6

3.2 Difference between SR based on MHI method and that based on the best estimated parameters

In MHI method, the Connor's constant and damping ratio are evaluated conservatively because lower bounded data are used for some parameters. The difference between the stability ratio based on MHI method and that based on the best estimated parameters is evaluated by the following equation.

$$R^{*}_{MHI} = \frac{SR_{MHI}}{SR_{BE}} = \frac{\frac{1}{K_{MHI}\sqrt{\zeta_{MHI}}} \cdot \overline{SR^{*}_{MHI}}}{\frac{1}{K_{BE}\sqrt{\zeta_{BE}}} \cdot \overline{SR^{*}}} = \frac{K_{BE}}{K_{MHI}}\sqrt{\frac{\zeta_{BE}}{\zeta_{MHI}}} \cdot \frac{\overline{SR^{*}_{MHI}}}{\overline{SR^{*}}} \quad \cdots\cdots (5)$$

Where,

R^{*}_{MHI} : Relative stability ratio based on MHI evaluation method
SR_{MHI} : Stability ratio based on MHI evaluation method
SR_{BE} : Mean stability ratio based on the best estimated parameters
K_{MHI} : Connor's constant based on MHI evaluation method
K_{BE} : Mean Connor's constant based on the best estimated parameters
ζ_{MHI} : Damping ratio based on MHI evaluation method
ζ_{BE} : Mean damping ratio based on the best estimated parameters
$\overline{SR^{*}}$: Average of normalized SR based on three different TH codes (See Sec. 4.2)
$\overline{SR^{*}_{MHI}}$: Average of normalized SR based on MHI-ATHOS (See Sec. 4.2)

When the relative ratio of Connor's constant and damping ratio are defined as shown in equation (6) and (7), equation (5) is converted to equation (9).

$$R_K = \frac{K_{MHI}}{K_{BE}} \quad \cdots\cdots (6)$$

$$R_\zeta = \frac{\zeta_{MHI}}{\zeta_{BE}} \quad \cdots\cdots (7)$$

$$R_{TH} = \frac{\overline{SR^{*}_{MHI}}}{\overline{SR^{*}}} \quad \cdots\cdots (8)$$

$$R^{*}_{MHI} = \frac{1}{R_K}\sqrt{\frac{1}{R_\zeta}} \cdot R_{TH} \quad \cdots\cdots (9)$$

Based on Table 2, the relative ratios of Connor's constant and damping ratio are converted to Equation (10) and (11).

$$R_K = \frac{K_{MHI}}{K_{BE}} = \frac{K1_{MHI}}{K1_{BE}} \cdot \frac{a(\theta)_{MHI}}{a(\theta)_{BE}} \quad \cdots\cdots (10)$$

$$R_\zeta = \frac{\zeta_{MHI}}{\zeta_{BE}} = \frac{\zeta_{TP}\frac{\zeta_{TP-MHI}}{\zeta_{TP-BE}} + \zeta_{SF}\frac{\zeta_{SF-MHI}}{\zeta_{SF-BE}}}{\zeta} \quad \cdots\cdots (11)$$

Where,

$K1_{MHI}$: Connor's constant based on MHI evaluation
$K1_{BE}$: Mean Connor's constant based on the experimental data
$a(\theta)_{MHI}$: The effect of flow direction based on MHI evaluation method
$a(\theta)_{BE}$: Mean effect of flow direction based on the experimental data
ζ_{SF-MHI} : Squeeze film damping ratio based on MHI evaluation method
ζ_{SF-BE} : Mean squeeze film damping ratio based on the experimental data
ζ_{TP-MHI} : Two phase damping ratio based on MHI evaluation method
ζ_{TP-BE} : Mean two phase damping ratio based on the experimental data

3.3 Uncertainty of SR

Based on the standard deviation and the relative stability ratio, the uncertainty of stability ratio based on the MHI method is obtained from the following equations.

For the upper bound,

$$\frac{SR_{\max}}{SR_{MHI}} = \frac{1+2\sigma_{SR}}{R^*_{MHI}} \quad \cdots\cdots (12)$$

For the lower bound,

$$\frac{SR_{\min}}{SR_{MHI}} = \frac{1-2\sigma_{SR}}{R^*_{MHI}} \quad \cdots\cdots (13)$$

Table 2 Parameters used for SR calculation

Parameter			Consideration	Basis
U_e		Effective flow velocity	Yes	The uncertainty of these parameters due to thermal-hydraulic parameters analysis error is evaluated by the comparison of three independent analyses as shown in Section 4.2.
U_c		Critical flow velocity	Yes	
f		Tube natural frequency	Yes	
m_0		Average tube mass	Yes	
ρ_0		Fluid density	Yes	
K (See Sec.4.1 (1))	$K1$	Connors's constant based on MHI test	Yes	The uncertainty of $K1$ is estimated based on MHI test data.
	K_p	The coefficient to consider the effect of tube pitch on K	No	Lower limit of Pettigrew's test data is used for SR calculation. (Ref. 4) It is not necessary to consider uncertainty of K_p
	κ	The ratio of K in the in-plane FEI to that of the out-of–plane FEI	No	The result of MHI air flow test was consistent with the public test data (See Sec. 7.1.1.2 (3) of main report). Therefore the uncertainty of κ is not necessary to consider.
	$a(\theta)$	The coefficient to consider the effect of flow angle on K	Yes	Lower limit of Yeung's test data is used for SR calculation. (Ref. 1) The uncertainty of $a(\theta)$ is estimated based on test data.
ζ (See Sec.4.1 (2))	ζ_{ST}	Structural damping ratio	No	ζ_{ST} is relatively small compared to ζ_{SF}
	ζ_{TP}	Two-Phase damping ratio	Yes	The uncertainty of ζ_{SF} is estimated based on Prof. Pettigrew's test data.
	ζ_V	Viscous damping ratio	No	ζ_V is not used for SR calculation
	ζ_{SF}	Squeeze film damping ratio	Yes	The uncertainty of ζ_{SF} is estimated based on Prof. Pettigrew's test data.

4. Evaluation Result

4.1Parameters Used for SR Evaluation

(1) Connors' constant

Connor's constant based on MHI test

Standard Deviation of Connors' constant K is estimated based on MHI's steam water two phase flow test data to investigate the fluid elastic vibration in the out of plane direction. 6

Figure 1 shows Connors' constant data obtained by MHI's test (black points • in Figure 1). However Connors' constant data include the error due to estimating it without considering measuring error of ratio of volume flow rate, flow velocity and fluid density. Therefore it is necessary to consider the error of both ratio of volume flow rate β and Connors' constant K which are horizontal and vertical axis (these data are indicated as red points ■ in Figure 1). Equations for calculating the error are as follows. Here the effect of error of damping ratio on Connors' constant K is neglected. Because damping ratio is determined with shape of the spectrum, therefore it is assumed that estimation of damping ratio is not affected by measuring error.

・Error of Connors' constant

$$\varepsilon_K = \sqrt{\varepsilon_{Uc}^2 + \left(\frac{1}{2}\varepsilon_{m0}\right)^2 + \left(\frac{1}{2}\varepsilon_{\rho 0}\right)^2} \quad \cdots\cdots(14)$$

Where, Equation of Connors' constant : $K = \left(\frac{U_c}{fD}\right)\left(\frac{m_0\delta}{\rho_0 D^2}\right)^{-\frac{1}{2}}$

ε_K : Relative error of Connors' constant K

ε_{Uc} : Relative error of critical flow velocity

ε_{m0} : Relative error of tube density considered added mass of outside water

$\varepsilon_{\rho 0}$: Relative error of fluid density $(=\varepsilon_{m0})$

・Error of ratio of volume flow rate

$$\varepsilon_\beta = \frac{U_l}{U_g + U_l}\sqrt{\varepsilon_{Ug}^2 + \varepsilon_{Ul}^2} \quad \left(\varepsilon_\beta \beta = \frac{1}{(U_g + U_l)^2}\sqrt{U_l^2(\varepsilon_{Ug}U_g)^2 + U_g^2(\varepsilon_{Ul}U_l)^2} \right) \quad \cdots(15)$$

Where, Equation of ratio of volume flow rate : $\beta = \frac{U_g}{U_g + U_l}$

U_g : flow velocity of vapor (gas)

U_l : flow velocity of water (liquid)

ε_β : Relative error of ratio of volume flow rate

ε_{Ug} : Relative error of flow velocity of vapor (gas)

ε_{Ul} : Relative error of flow velocity of water (liquid)

According to MHI's test data, measuring error (ε_{Ug} , ε_{Ul} , ε_{m0} and $\varepsilon_{\rho 0}$) is as follows:

ε_{Ug} =| |

ε_{Ul} =| |

ε_{Uc} =| |(max value of measuring error of flow velocity; max(ε_{Ug} , ε_{Ul}))

$\varepsilon_{m0} = \varepsilon_{\rho 0}$ =| |(maximum value of measuring error of fluid density)

Measuring error of each parameter is estimated based on proof reading result and inspection result according to GUM (Guide to the expression of Uncertainty in Measurement, ASME).

Table 3 Measuring error of each parameter

	steam	water	
measuring error of pressure (%)			
fluid density at reference pressure; 6MPa (kg/m^3)			
fluid density at the pressure considering error; 6.02MPa (kg/m^3)			
measuring error of fluid density (%)			※1
measuring error of flow rate (%)			※2
measuring error of cross section (%)			※3
measuring error of flow velocity (%)			※4

※1 Relative error between fluid density at| |and| |

steam : | |

water : | |

※2 Proof reading result of flow rate measurement

※3 Measuring error of cross section is estimated by dimensional inspection result and measuring error of digital vernier calipers| |

※4 Measuring error of flow velocity is calculated by following equation in accordance with GUM

$$\varepsilon_U = 2 \times \sqrt{\frac{\varepsilon_Q^2}{3} + \frac{\varepsilon_A^2}{3} + \frac{\varepsilon_\rho^2}{3}}$$

Where

ε_U : measuring error of flow velocity

ε_Q : measuring error of flow rate

ε_A : measuring error of cross section

ε_ρ : measuring error of fluid density

steam : [ ]

water : [ ]

Therefore relative error of Connors' constant is estimated to be ε_K = [ ] by using equation (14). Also ε_β is calculated with measuring error ε_{Ug} & ε_{Ul} by using equation (15), the calculation result is shown in Table 4. Both relative error of ε_K and ε_β are calculated according to error propagation law. 6

Table 4 Calculation of relative error of β

β	jg+jl※1(m/s)	jg※2(m/s)	jl※2 (m/s)	ε_β (%)
0.7				
0.8				
0.9				
0.93				
0.98				

※1 Critical flow velocity obtained by MHI test [ ]

※2 Critical flow velocity of vapor and water calculated by test condition (linear interpolation)

Then the uncertainty of $K1$ is estimated from the measuring error of test data by calculating the maximum relative error of each data (red points ■ in Figure 1(a)) from fitting curve of original data. There are following 4 types of data when considering relative error of Connors' constant ($\pm\varepsilon_K$) and ratio of volume flow rate (v ε_β), because each relative error has positive and negative value (±ε).

(1) Data with $+\varepsilon_K$ and $+\varepsilon_\beta$

(2) Data with $+\varepsilon_K$ and $-\varepsilon_\beta$

(3) Data with $-\varepsilon_K$ and $+\varepsilon_\beta$

(4) Data with $-\varepsilon_K$ and $-\varepsilon_\beta$

There are data for uncertainty evaluation (red points ■ in Figure 1(a)) 4 times as much as test data (black points lue (±ε). wing 4 types of data when $K1$ is estimated by following equation as maximum relative error from fitting curve.

$$\varepsilon_{K1} = \max\left|\frac{K_i - \hat{K}}{\hat{K}}\right| \quad \cdots\cdots(16)$$

Where

K_i : each data for uncertainty evaluation ; $K1$

$\hat{K}$: approximate value at each β (fitting curve)

N : Number of data for uncertainty evaluation (4 times as much as test data)

Therefore, the standard deviation of $K1$ is assumed to be maximum relative error of all data (1)~

(4) at each ratio of volume flow rate ; $2\sigma_K = \varepsilon_{K1} =$ [ ] ($\sigma_K =$ [ ]). Because measuring error of $K1$ and β are estimated as 2 times as large as standard deviation : 2σ, it is assumed that $2\sigma_K = \varepsilon_{K1}$.

Since the mean data is used for the SR evaluation, the relative ratio of K1, $\frac{K1_{MHI}}{K1_{BE}}$, is [ ]

[ ]

Figure 1 Experimental data of Connors's constant based on MHI test ; $K1$

Effect of flow direction

Figure 2 shows Yeung's test data of the coefficient to consider the effect of flow angle on K; $a(\theta)$. Lower limit of the data is used for the stability ratio evaluation when the flow direction is smaller than 20 degrees; the flow directions are smaller than 20 degrees in the center of the bundle (FEI susceptible region) as shown in Figure 3.

In accordance with Figure 2, the standard deviation below 20 degrees is obtained to be [ ] and the mean line is added, which is [ ] larger than the lower limit used for the SR evaluation. Therefore, the relative ratio, $\frac{a(\theta)_{MHI}}{a(\theta)_{BE}}$, is [ ]

Connor's constant

Therefore, the standard deviation of Connor's constant, σ_K, is [ ] obtained by using Equation (4) and the relative Connor's constant, R_K, is [ ] obtained by using Equation (10) as follows.

$$\sigma_K = \sqrt{\sigma_{K1}^2 + \sigma_a^2} = [\quad]$$

$$R_K = \frac{K1_{MHI}}{K1_{BE}} \cdot \frac{a(\theta)_{MHI}}{a(\theta)_{BE}} = [\quad]$$

Figure 2 Experimental data of $a(\theta)$

Figure 3 Region where the flow direction is greater than 20 degrees from the tube in-plane direction to out-of-plane direction

(2) Damping Ratio

Squeeze film damping

Uncertainty of squeeze film damping ζ_{SF} is estimated based on Pettigrew's test data as shown in the Figure 4 (See Ref. 2). According to this figure, the squeeze film damping ratio depends on the vibration frequency and the bounded line of ζ_{SF}, with 90th percentile (= 50 / f) is used for the OA evaluation in accordance with Pettigrew's guideline.

As shown in Figure 4, the bounded line based on 90th percentile (= 50 / f) is used for MHI's SR evaluation. In order to obtain the standard deviation and the relative ratio, the lower bounded line with 95th percentile (= 43.5 / f) and the average line (= 100 / f)are added.

Since the difference between 95th percentile and the average line is considered as $2\sigma_{SF}$, the standard deviation is [ ] and the ratio between 90th percentile and the average line is the relative ratio of squeeze film damping, $\frac{\zeta_{SF-MHI}}{\zeta_{SF-BE}}$, which is [ ]

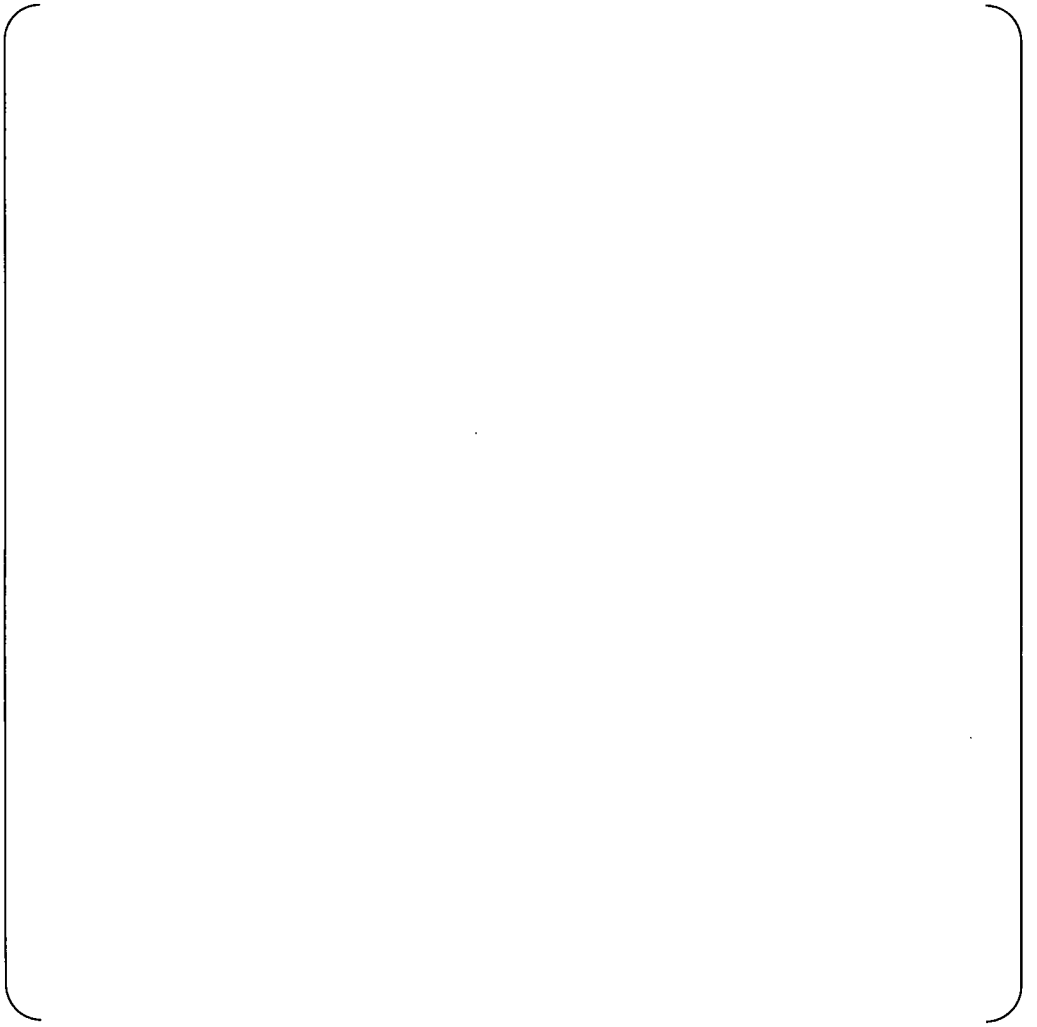

Note) because there are 20 points below the Pettigrew's guideline with 90th percentile, the lower bounded line with 95th percentile is determined such that there are 10 plot points below this line

Figure 4 Experimental data of squeeze film damping

Two phase damping

Uncertainty of two phase damping ζ_{TP} is estimated based on Pettigrew's test data as shown in Figure 5 (See Ref. 5). In order to obtain the standard deviation and the relative ratio, the lower bounded line of all the data, which is assumed to show 99. 7th percentile (= -3a_{TP}), is added. Since the difference between the gradient of the 99.7th percentile | | and the gradient of the average line | | is considered as 3s_{TP}, the standard deviation is | | The ratio between the gradient of guide line used for SR evaluation | | and the gradient of the average line | | is the relative ratio of two phase damping, $\frac{\zeta_{TP-MHI}}{\zeta_{TP-BE}}$, which is | | 6

[ ]

Figure 5 Experimental data of two phase damping

Total damping ratio

According to equation (3), in order to estimate the standard deviation of total damping ratio ζ, it is necessary to consider absolute value of each damping ratio. According to damping ratio data used in analysis shown in Table 5, it is found that $\zeta_{SF}/\zeta =$ | | and $\zeta_{TP}/\zeta =$ | | Therefore the standard deviation of total damping ratio, σ_ζ, is estimated to be | | as follows.

$$\sigma_\zeta = \frac{\sigma_{SF}\zeta_{SF} + \sigma_{TP}\zeta_{TP}}{\zeta} = \left| \quad \right|$$

The relative damping ratio is obtained to be | | by using Equation (11) as follows.

$$R_\zeta = \frac{\zeta_{SF}\dfrac{\zeta_{SF-MHI}}{\zeta_{SF-BE}} + \zeta_{TP}\dfrac{\zeta_{TP-MHI}}{\zeta_{TP-BE}}}{\zeta} = \left| \quad \right|$$

4.2 SR due to Thermal-Hydraulic Parameters Evaluation

In order to evaluate the standard deviation of SR due to the thermal-hydraulic (TH) parameters evaluation, stability ratios for representative 8 tubes are calculated by using 3 independent TH analysis codes (MHI-ATHOS, CAFCA and WEC-ATHOS)

Table 5 shows the results of SR calculation and the normalized values, which are the ratio between the calculated SRs based on each TH analysis and the average of SRs based on 3 analysis codes. The standard deviation of normalized stability ratios obtained by the following equation is [ ] and the average relative stability ratio based on MHI ATHOS is [ ] 6

$$\sigma_{TH} = \sqrt{\frac{1}{N} \cdot \sum_{i}^{N} \left(\frac{SR_i^* - \overline{SR^*}}{\overline{SR^*}} \right)^2} \quad \cdots\cdots (17)$$

Where,

σ_{TH} : Standard deviation of SR based on each TH code

SR^* : Normalized SR (= each analysis result / average value of 3 analysis code result)

$\overline{SR^*}$: Average of normalized SR

N :Number of data

Table 5 Comparison of Stability Ratio based on MHI-ATHOS, CAFCA and WEC-ATHOS

Row	Column	MHI-ATHOS		CAFCA		WEC-ATHOS		Average	
		SR	Normalized SR	SR	Normalized SR	SR	Normalized SR	SR	Normalized SR
81	69								
81	89								
101	69								
101	89								
121	69								
121	89								
125	85								
105	69								
Average									

4.3 Uncertainty of SR

Table 6 shows the standard deviation and the relative ratio of each parameter. According to equation (2), the standard deviation of stability ratio is calculated to be[ ]as follows. 6

$$\sigma_{SR} = \sqrt{\sigma_K^2 + \left(\frac{1}{2}\sigma_\varsigma\right)^2 + \sigma_{TH}^2} = \left[\quad\right]$$

The upper bounded and lower bounded of stability ratios are -5% and -57%, which are obtained by Equation (12) and (13).

Table 6 Uncertainty of Stability Ratio 6

Parameters		Relative Ratio based on MHI method	Best estimated		Uncertainty of MHI's SR evaluation	
			Mean	σ	Upper bound $\frac{SR_{max}}{SR_{MHI}}$	Lower bound $\frac{SR_{min}}{SR_{MHI}}$
Connor's constant	K1					
	$a(\theta)$					
	K					
Damping Ratio	ζ_{SF}					
	ζ_{TP}					
	ζ					
Thermal-Hydraulic Parameters						
Stability Ratio						

5. References

[1] "The Effect of Approach Flow Direction on the Flow-Induced Vibrations of a Triangular Tube Array" , H.C. Yeung et al, 1983, Transactions of the ASME Vol.105

[2] "ransactions of the ASHEAT EXCHANGER TUBES: PART2: IN LIQUIDS" , M.J.Pettigrew et al.

[3] "Advanced Estimation on Fluidelastic Instability U-bend Tube Bundle of Steam Generator (3rd Report, Advanced Estimated Method)St, 2002, T. Nakamura et al, Journal of The Japan Society of Mechanical Engineers Vol 63 Issue 668

[4] 3 Issue 668of tube bundle geometry on vibration in two-phase cross flowor, 2000, M. J. Pettigrew et al, Flow Induced Vibration, Ziada & Staubli (eds) © 2000 Balkema, Rotterdam, ISBN 90 5809 129 5, 561-568

[5] "Vibration analysis of shell-and-tube heat exchangers : an overview – Part1: flow, damping, fluid elastic instability ", 2003, M.J. Pettigrew et al, Journal of Fluids and Structures 18 469-483

Attachment-7 Selection of Evaluated Tubes

As shown in Table 1, 28 tubes are selected for thermal hydraulic analysis by ATHOS/SGAP (see Ref.21 for detail). Among these tubes, 8 tubes (#2,#3,#6,#7,#10,#11,#14,#16) selected by SCE (See the emails shown in Appendix-1) and an additional tube (#28), which stability ratio of out-of-plane FEI was the maximum when all AVB support points are active, are evaluated in the main report. △6

Table 1 Evaluated Tubes (See Ref.22 for details)

Tube #	Row	Column
1	80	60
2*1	80	70
3*1	80	80
4	80	88
5	100	60
6*1	100	70
7*1	100	80
8	100	88
9	120	60
10*1	120	70
11*1	120	80
12	120	88
13	80	84
14*1	95	85
15	110	84
16*1	125	85
17	135	85
18	40	30
19	74	80
20	95	69
21	105	69
22	111	69
23	127	73
24	138	80
25	86	80
26	95	75
27	124	76
28*2	138	84

Notes:

(*1) Representative tubes for evaluating stability ratio selected by SCE

(*2) Selected as an additional representative tube because the stability ratio of out-of-plane is the maximum when all AVB support points are active

△6

Appendix-1 E-mails from SCE

[ ]

6

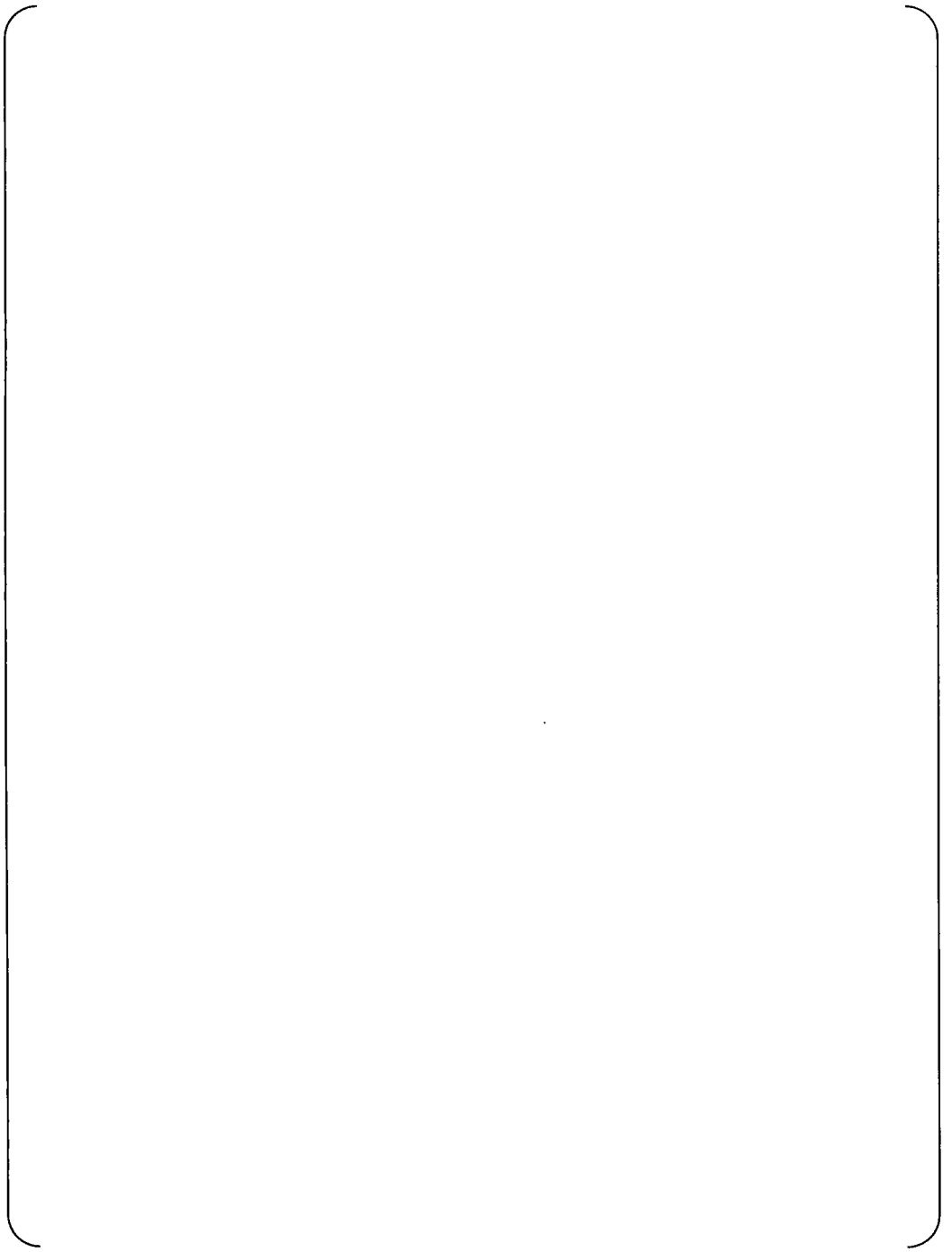

6

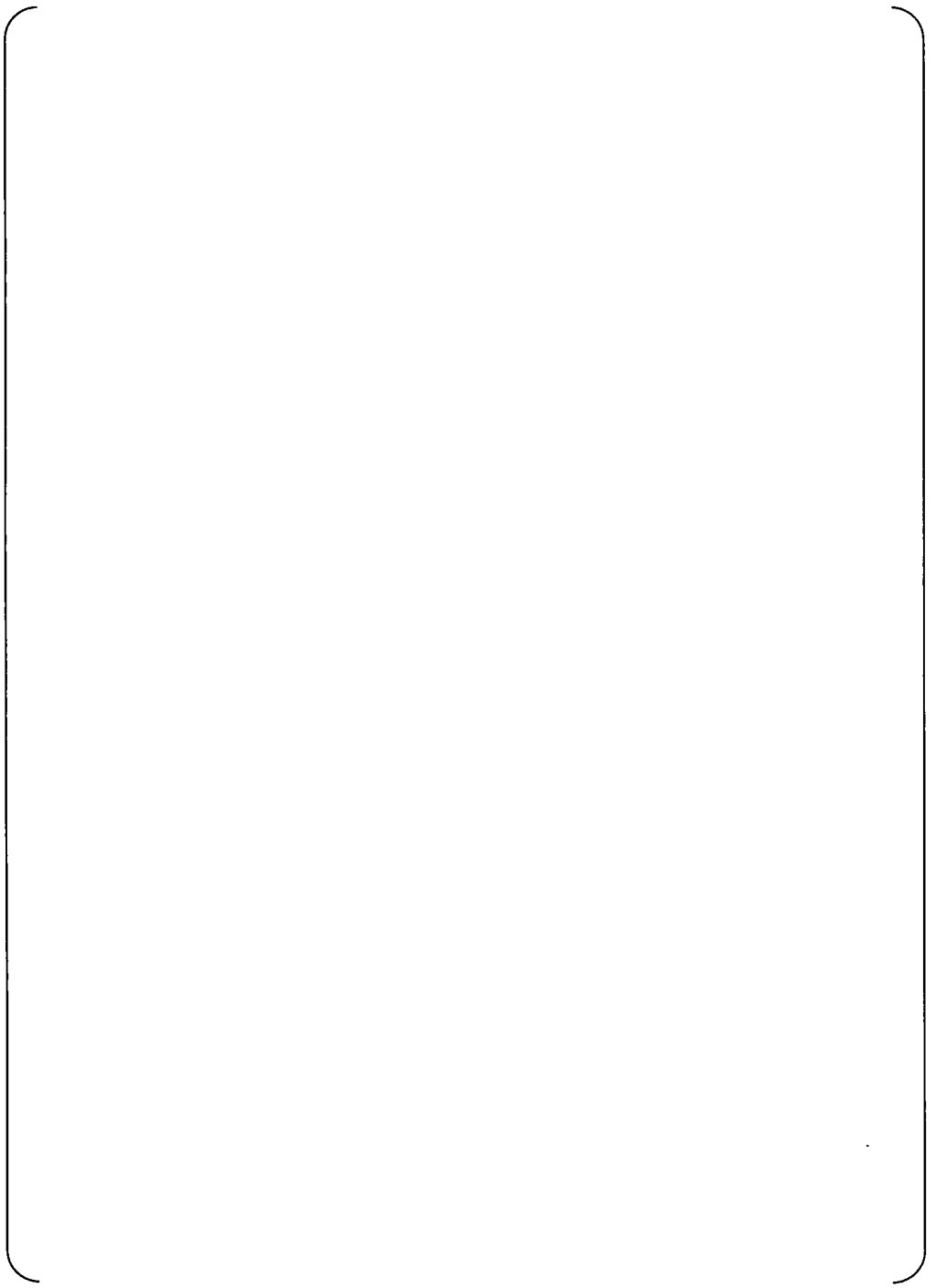

6